

Journal of Taibah University for Science



ISSN: 1658-3655 (Online) Journal homepage: www.tandfonline.com/journals/tusc20

Comparative mechanistic study of greensynthesized silver-zinc oxide (Ag-ZnO) and iron-Zinc oxide (Fe-ZnO) bimetallic nanoparticles in antiglycation, antidiabetic, antioxidant, and anticancer activities

Sumaira Anjum, Mubashra Inam, Amar Yasser Jassim, Iqra Attique, Maryam Zahra, Fayez Althobaiti, Mohamed Mohamed Soliman, Khalid S. Alotaibi, Shatha B. Albattal & Christophe Hano

To cite this article: Sumaira Anjum, Mubashra Inam, Amar Yasser Jassim, Iqra Attique, Maryam Zahra, Fayez Althobaiti, Mohamed Mohamed Soliman, Khalid S. Alotaibi, Shatha B. Albattal & Christophe Hano (2025) Comparative mechanistic study of green-synthesized silver-zinc oxide (Ag-ZnO) and iron–Zinc oxide (Fe-ZnO) bimetallic nanoparticles in antiglycation, antidiabetic, antioxidant, and anticancer activities, Journal of Taibah University for Science, 19:1, 2515712, DOI: 10.1080/16583655.2025.2515712

To link to this article: https://doi.org/10.1080/16583655.2025.2515712

9	© 2025 The Author(s). Published by Informa UK Limited, trading as Taylor & Francis Group.	+	View supplementary material 🗹
	Published online: 05 Jun 2025.		Submit your article to this journal 🗗
hil	Article views: 687	Q ¹	View related articles 🗷
CrossMark	View Crossmark data ☑		









Comparative mechanistic study of green-synthesized silver-zinc oxide (Ag-ZnO) and iron–Zinc oxide (Fe-ZnO) bimetallic nanoparticles in antiglycation, antidiabetic, antioxidant, and anticancer activities

Sumaira Anjum^a, Mubashra Inam [©]a,b, Amar Yasser Jassim^c, Iqra Attique^a, Maryam Zahra^a, Fayez Althobaiti ^{od}, Mohamed Mohamed Soliman ^{oe}, Khalid S. Alotaibi ^{of}, Shatha B. Albattal ^{of} and Christophe Hano⁹

^aDepartment of Biotechnology, Kinnaird College for Women, Lahore, Pakistan; ^bDepartment of Biochemistry and Molecular Biology, Faculty of Medicine, University of Debrecen, Debrecen, Hungary; CMarine Science Center, University of Basrah, Basrah, Iraq; Department of Biotechnology, College of Science, Taif University, Taif, Saudi Arabia; eClinical Laboratory Sciences Department, Turabah University College, Taif University, Taif, Saudi Arabia; fGeneral Science and English Language Department, College of Applied Sciences, AlMaarefa University, Riyadh, Saudi Arabia; ⁹Department of Chemical Biology, Eure & Loir Campus, University of Orleans, France

ABSTRACT

Bimetallic nanoparticles (BNPs) have gained immense attention for their diverse biological applications. This study aimed to biosynthesize and characterize Aq-ZnONPs and Fe-ZnONPs and compare their potential as therapeutic agents. The BNPs were synthesized using Mentha asiatica plant extract and characterized using various techniques such as UV-visible spectroscopy, TEM, EDX spectroscopy, ATR-FTIR spectroscopy, PXRD, DLS, and zeta potential analyses. TEM, EDX, and XRD revealed the structural and morphological properties of crystalline Ag-ZnONPs and Fe-ZnONPs. FTIR analysis investigated the plant phytochemicals responsible for the stabilization and capping of BNPs. Ag-ZnONPs showed higher biocompatibility than Fe-ZnONPs. Fe-ZnONPs exhibited-significantly higher anticancer potential than Ag-ZnONPs as evident by Reactive Oxygen Species/ Nitric Oxide Synthase production, along with cell viability analysis, loss of mitochondrial-membrane potential, enhanced caspase-3 gene-expression, and intensified activity of Caspase-3/7. Collectively, our findings underscore the promising therapeuticpotential of BNPs in cancer treatment and diabetes, setting them as strong candidates for future biomedical applications.

ARTICLE HISTORY

Received 23 December 2024 Revised 28 May 2025 Accepted 31 May 2025

KEYWORDS

Mentha asiatica; bimetallic nanoparticles; silver-zinc oxide and iron-zinc oxide; anticancer; antidiabetic and antiglycation; antioxidant

1. Introduction

Bimetallic nanoparticles (BNPs) have become valuable in recent years due to their enhanced optical, electronic, magnetic, and catalytic properties [1,2]. The synergistic effects between two metal components lead to improved stability, increased surface area, and enhanced reactivity, which makes BNPs superior to their monometallic counterparts [3]. As they are formed by combining two distinct metal types, the resulting structures range from alloy and intermetallic particles to core-shell and multi-shell configurations. Many kinds of BNPs synthesized with the integration of zinc oxide nanoparticles (ZnONPs), such as Au-ZnO, Ag-ZnO, Cu-ZnONPs, and Fe-ZnONPs, have been reported in the literature [4-6]. However, the properties and performance of BNPs are highly dependent on the choice of metals, their ratio, and the method used for their synthesis [7]. Given that, we used a plant-based synthesis method utilizing Mentha asiatica leaf extract. It is rich in

bioactive compounds such as phenols, flavonoids, and terpenoids, and exhibits immense biological and therapeutic properties [8,9]. These compounds not only facilitate the reduction and stabilization of nanoparticles but may also enhance their therapeutic efficacy.

Green-synthesized nanoparticles offer a multitude of advantages over their chemically generated counterparts. To begin with, green synthesis encompasses the fundamental benefits of sustainable, non-toxic, environmentally friendly, cost-effective, and scalable products [10]. Moreover, the process itself is quite simple and can be monitored in real time [11]. Recent reports further support these advantages, where plantbased extracts have successfully facilitated the synthesis of biologically active nanoparticles, such as using Cotoneaster nummularia under diffused sunlight for wound healing applications, or olive fruit extract for generating antioxidant and antibacterial AgNPs [12,13]. Some of the most pertinent advantages lie in the field of

CONTACT Sumaira Anjum 🔯 sumaira.anjum@kinnaird.edu.pk 📵 Department of Biotechnology, Kinnaird College for Women, 93-Jail Road, Lahore

Supplemental data for this article can be accessed online at https://doi.org/10.1080/16583655.2025.2515712.

medicine, as the nanoparticles, being capped by natural biomolecules, not only ensure biocompatibility, but the functionalization potential also enhances nanoparticle activity and stability [14-16]. For these reasons, green synthesized nanoparticles are routinely employed in targeted drug delivery, gastroprotective activities, cancer treatment, magnetic resonance imaging (MRI), gene therapy, and as biosensors and anti-microbial agents [17,18].

The bimetallic nanostructures have improved effectiveness and enhanced biocompatibility, paving the way for biomedical applications. One of the potential applications of BNPs is their antidiabetic action. The regulatory potential of selenium-based nanomaterials in managing diabetes through modulation of selenoproteins has been reported recently [19]. Ag-ZnONPs have been reported to exhibit inhibitory properties against amylases and glucosidases [4]. The antidiabetic activity has been observed in its monometallic counterparts, however, the synergistic action of Fe-ZnONPs has not been reported in the literature so far [20,21]. Other promising applications of BNPs include antiglycation and antioxidant activities. BNPs such as Au-ZnONPs and Fe-ZnONPs have been reported to increase the levels of antioxidant enzymes such as superoxide dismutase (SOD) and catalase (CAT) [22,23]. Moreover, these BNPs have been extensively studied for their inhibitory action against advanced glycation end products (AGEs), making them a potential therapeutic candidate for agerelated disorders [24]. Furthermore, they offer significant anticancer potential and have been reported to be effective against various cancerous cell lines by direct application and as nanocarriers [25,26]. In addition, BNPs such as platinum-iron and Fe-ZnONPs have also been studied for sonodynamic cancer therapies and have produced favourable results [27,28]. The current study utilized cell-free assays and HepG2 cell lines to study the above-discussed applications of Ag-ZnONPs and Fe-ZnONPs.

Developing novel BNPs with enhanced therapeutic potential is crucial to advancing treatment strategies in various biomedical fields. Despite the significant progress, a gap still exists in the knowledge regarding the comparative potential of Ag-ZnONPs and Fe-ZnONPs, particularly in terms of their anti-diabetic, antiglycation, antioxidant, and anticancer activities. The rationale behind this study stems from the need to investigate and compare the therapeutic efficiencies of these two BNPs systems, as their distinct metal combinations can lead to differences in performance. Specifically, Fe-ZnONPs are hypothesized to exhibit unique synergistic effects that have not been thoroughly explored, particularly in inhibiting key enzymes related to diabetes, oxidative stress management, and cancer treatment. The current study aims to uncover the biomedical activities of Ag-ZnONPs and Fe-ZnONPs and provide mechanistic insights as to how they exhibit certain actions to advance their use in therapeutic applications.

2. Materials and methods

2.1. Preparation of M. asiatica leaf extract

Bundles of freshly grown *M. asiatica* (Accession number: 433489) leaves were harvested from the local farms during the late summer in August. Ten grams of leaves were washed with tap and distilled water to remove impurities. The leaves were then cut into smaller pieces, added to 400 mL of distilled water in a beaker, and heated to 200°C until the volume was reduced to 100 mL. The mixture was subsequently ground for 2 min and filtered using Whatmann filter paper No. 1. The resulting plant extract (PE) was stored at 4°C until further use for BNPs synthesis and phytochemical investigations.

2.2. Analysis of phytochemical constituents

Phytochemical Analysis was performed in terms of total phenolic content (TPC) and total flavonoid content (TFC). Folin-Ciocalteu's test, developed by Anjum et al. was conducted to investigate TPC [29]. The UV-visible spectrophotometer (Specord-200, Analytik Jena, Germany) was used to measure the absorbance of the samples at 750 nm. TPC was reported in terms of mg of Gallic Acid Equivalent (GAE)/g dry weight of PE, and gallic acid was set as a standard. Likewise, TFC was determined using the aluminium chloride colorimetric method as defined by Naqvi et al., followed by measuring absorbance at 415 nm [30]. Quercetin was used as a standard, and results were reported as mg of quercetin/g dry weight.

2.3. Free radical scavenging activity (FRSA)

The antioxidant potential of PE was determined using 2, 2-diphenyl-1-picrylhydrazyl (DPPH). For this purpose, the method of Inam et al. was employed for measurement and calculations [31]. UV-vis spectrophotometer was used to measure the absorbance of the reaction mixture at 517 nm. The experiment was performed in triplicates.

2.4. Biosynthesis of BNPs

PE-assisted synthesis of Ag-ZnONPs was executed following the modified method of Anjum et al [4]. 1 mL of PE and 50 mL of 0.5 M zinc acetate solution were heated at 60°C for 5 mins. Then, 10 mL of 0.1M silver nitrate was added, and the pH was adjusted to 9 with 1 M NaOH. The solution was stirred at 60°C for 2 h. The resulting precipitates were allowed to settle and micro-centrifuged at 13000 rpm for 15 min. The pellets obtained were placed in an incubator at 30°C for 24 h to allow them to dry completely. Lastly, the dried product was crushed to a

fine powder using a pestle and mortar. The synthesized Ag-ZnONPs were collected in a microtube, labelled, and stored for further usage.

Fe-ZnONPs were synthesized by following Reyes-Pérez et al. with slight modifications [32]. 50 mL of 0.5 M zinc acetate solution and 20 mL of 0.02 M iron sulphate solution were prepared, and a reduction reaction was carried out in two steps. Following the first step as in Ag-ZnONPs synthesis, the resulting mixture of PE and zinc acetate solution was added to 20 mL of iron sulphate solution. The mixture was stirred continuously for 1 h and then allowed to rest for 24 h. The mixture was subjected to further treatments under conditions like Ag-ZnONPs.

2.5. Characterization of BNPs

Structural and physicochemical characterization was carried out by using various techniques such as UV-vis Spectrophotometry, Transmission Electron Microscopy (TEM), Energy Dispersive X-ray (EDX) Analysis, Attenuated Total Reflection-Fourier Transform Infrared (ATR-FTIR) Spectroscopy, Powdered X-Ray Diffraction (PXRD), Dynamic Light Scattering (DLS), and Zeta Potential analysis.

UV-vis Spectrophotometer was used to record the synthesis and stability of BNPs. Transmission Electron Microscope (JEM-2100, JEOL Ltd., Japan) was used to evaluate the shape of BNPs and to determine their estimated size. The procedure outlined by Faisal et al. was used to prepare samples and take TEM micrographs [33]. EDX analysis was performed using an EDX detector coupled with TEM to ascertain the elemental composition of BNPs. ATR-FTIR Spectroscopy (VERTEX 70v FT-IR Spectrometer, United States) was used to determine the functional groups of the phytochemicals responsible for coating and stabilizing BNPs. The peaks between 650 and 4000 cm⁻¹ were recorded. The crystalline structure of BNPs was determined using Powdered X-ray Diffractometer (AXS DS Advance, Bruker, USA) following the conditions of Inam et al., and the crystalline size of BNPs was determined using Debye-Scherrer's formula (D = $k\lambda/\beta\cos\theta$) [31]. The size distribution and zeta potential of BNPs were calculated by applying DLS using Zetasizer (Malvern, NanoZSP, UK) following the method of Sohail et al [34].

2.6. Biocompatibility analysis of BNPs

Brine shrimp lethality analysis and hemo-compatibility analysis using RBCs were performed to analyse the biocompatibility of BNPs. 100 µg/mL concentration of BNPs was used to conduct the biocompatibility studies based on the available literature for optimal experimental outcomes. The experiments were performed in triplicates following the protocol outlined by Inam et al [31]. Ethical standards of the International and National Research Committees and the 1964 Helsinki Declaration and its later amendments were duly considered while conducting the experiments, as human participants were involved in obtaining blood samples.

2.7. Antidiabetic and antiglycation potential of **BNPs**

The antidiabetic potential of Ag-ZnONPs and Fe-ZnONPs was determined against α -amylase and α glucosidase enzymes, as performed by Shah et al [35]. The enzymatic activity was measured at 405 nm, with % inhibition calculated. Similarly, the antiglycation activity of BNPs was measured in terms of vesperlysine-like (V-AGEs) and pentosidine-like AGEs (P-AGEs) inhibition following the protocol of Shah et al [35]. The quantity of formed AGEs was measured using fluorescence (Versa Fluor fluorometer); Bio-Rad, Marnes-la-Coquette, France, set at wavelengths of 410 nm emission and 330 nm excitation, respectively. The inhibition of AGEs formation was expressed in terms of % inhibition relative to the control.

2.8. Antioxidant activities of BNPs

The antioxidant capacity of Ag-ZnONPs and Fe-ZnONPs was measured using four assays. In the Oxygen Radical Absorbance capacity (ORAC) assay, 10 µL of the sample was mixed with fluorescein and ABAP as performed by Shah et al., and fluorescence was recorded over 2.5 h at 37°C [35]. The 2,2-Azinobis-3-ethylbenzthiazoline-6sulphonic acid (ABTS) assay was conducted by following the procedure of Inam et al., in which ABTS solution was mixed with samples, and absorbance was recorded at 734 nm after 15 mins in the dark. The Ferric Reducing Antioxidant Power (FRAP) analysis was performed following Abbasi et al.'s method, with the absorbance of the final reaction mixture recorded at 630 nm [36]. In the Cupric Reducing Antioxidant Capacity (CUPRAC) assay, samples were mixed with neocuproine, Cu (II), and acetate buffer was added, followed by incubation at 25°C, with absorbance recorded at 450 nm. It was carried out following the method of Apak et al [37]. All assays were performed thrice, and results were expressed as microMolar Trolox equivalent antioxidant capacity (µM TEAC).

2.9. Anticancer activity of BNPs

Following Meer et al. MTT (3-(4,5-dimethylthiazolyl-2)-2,5-diphenyltetrazolium bromide) assay was performed upon HepG2 human hepatoblastoma cell lines (ATCC HB-8065; USA) for assessing cell viability with non-treated cells (NTC) as control [38]. Optimized concentrations of Fe-ZnONPs and Ag-ZnONPs were employed, and all experiments were carried out in triplicate. In addition, membrane integrity analysis

of HepG2 cells was performed in terms of Reactive Oxygen Species/Nitric Oxide Synthase (ROS/NOS) production and Mitochondrial Membrane Potential (MMP). The method reported by Nazir et al. was employed to assess the intracellular ROS/NOS level by using dihydrorhodamine-123 (DHR-123) fluorescent dye (Sigma, Saint Quentin Falavier, France) [39]. The results were expressed in terms of relative fluorescence units (RFU). Loss of MMP in HepG2 cells as a result of BNPs' actions was determined using the method devised by Khan et al [40]. Cell culture was supplied with 25 nM 3,3'-dihexyloxacarbocyanine iodide following the incubation of cells at 37 °C for 40 min. The MMP was expressed as relative fluorescent units (RFU). The experiment was performed in triplicates. Furthermore, Caspase-3 gene expression and Caspase 3/7 Activity were measured in BNPs-treated HepG2 cells. To measure the expression of Caspase-3, the protocol and conditions pre-optimized by Anjum et al. were followed [29]. The results were expressed in the units of Log 2-fold Activity. Caspase 3/7 activity was estimated using the Apo-ONE Homogeneous Caspase-3/7 Assay kit (Promega, Charbonnières-les-Bains, France) following the instructions of the manufacturer. Three repetitions of the experiment were performed, and results were expressed in terms of RFU/mg Protein.

2.10. Graphical and statistical analyses

All the data were graphically and statistically evaluated by using Image J, OriginPro 8.5, Microsoft Excel 2019, and GraphPad Prism 8.0.2 software. The results of the experiments were expressed in terms of Mean \pm SD, followed by Paired Sample T-tests, One-way ANOVA, and Bonferroni multiple comparison tests (p < 0.05).

3. Results and discussion

3.1. Phytochemical analysis of M. asiatica leaf extract

Secondary metabolites, particularly phenolics and flavonoids, found in plant leaf extracts, are utilized as natural reducing and stabilizing agents and are crucial for the green synthesis of BNPs [41]. These compounds contribute significantly to the reduction of metal ions during nanoparticle synthesis and enhance the stability and bioactivity of the BNPs [7]. In this study, TPC and TFC of M. asiatica extract were determined to be 122.43 \pm 0.03 mg GAE/g DW and 91.48 \pm 0.76 mg QE/g DW, respectively. High phenolic and flavonoid content in M. asiatica aligns with the previous studies, where phytochemical-rich plants were utilized for NPs fabrication. Alharbi et al. revealed in their study that the total flavonoid and phenolic content of Ocimum sanctum was 82.02 ± 8.17 mg GAE/g and 74.6 ± 5.1 mg, respectively [42]. Moreover, Kashkoul et al. evaluated

the aqueous extract of Laurus nobilis leaves that are rich in flavonoids (21.576 \pm 0.0763 mg/L) and phenolic compounds (23.964 \pm 0.0698 mg/L), which effectively mediated the synthesis of stable NPs [43]. Compared to these studies, the higher phenolic content in M. asiatica suggests its superior potential in BNPs synthesis, likely enhancing the antioxidant and other bioactive properties of the fabricated nanoparticles. FRSA analysis of M. asiatica provided crucial insights regarding its antioxidant potential, and the results were expressed in terms of % of decolorization. The analysis showed $69.4 \pm 0.12\%$ of decolorization, demonstrating the high antioxidant potential of the plant extract. Our results are in harmony with Benabdallah et al., which showed high inhibitory activity of different *Mentha* species against DPPH [44].

3.2. Biosynthesis of BNPs

Many investigations and experiments have been descri bed in the literature on the green production of Ag-ZnONPs from different plant extracts, as they have been demonstrated to be remarkable bioreactors for producing NPs. Kyomuhimbo et al. biosynthesized bimetallic Aq-ZnONPs using the extract of Bidens pilosa [45]. Green synthesis of Aq-ZnONPs was accomplished by Hosny et al. using Persicaria salicifolia, and Thatoi et al. with extracts of Heritiera fomes and Sonneratia apetala [46,47]. In our study, bluish-grey Ag-ZnONPs pellets were obtained, and the highest yield was obtained after continuous stirring for 2 h. The dried pellets were then converted into powdered form using a pestle and mortar for further applications. The obtained yield of Ag-ZnONPs was 2 g BNPs: 1 ml PE: 50 ml Zinc acetate: 10 ml silver nitrate. In the case of Fe-ZnONPs, the best results were obtained after continuous stirring for 1 h. The resulting, black-colored pellets were isolated, dried, and converted into powdered form for future use. The obtained yield of Fe-ZnONPs was 4 g BNPs: 1 ml PE: 50 ml Zinc acetate: 20 ml Iron Sulphate. Our results are in harmony with those of Reyes-Pérez et al. where black-colored BNPs were obtained with zinc acetate and iron sulfate as salt precursors [32]. Jan et al. reported reddish-yellow Fe-ZnONPs when zinc nitrate and iron nitrate were used as salt precursors. This shows that the choice of salt precursors affects the physicochemical properties of the BNPs [48].

3.2.1. Probable mechanism for BNPs formation

The expected mechanism of the formation of Ag-ZnONPs involves the initial chelation of Zn²⁺ ions with the plant phytochemicals to form Zn-complex [49]. Upon adding AgNO₃, the same phytochemicals result in the reduction of Ag⁺ ions to Ag⁰. In basic and slightly heating conditions, zinc complex hydrolyzes and results in the formation of ZnO. Ag⁰ particles anchor or nucleate over the growing ZnO matrix, stabilized by plant

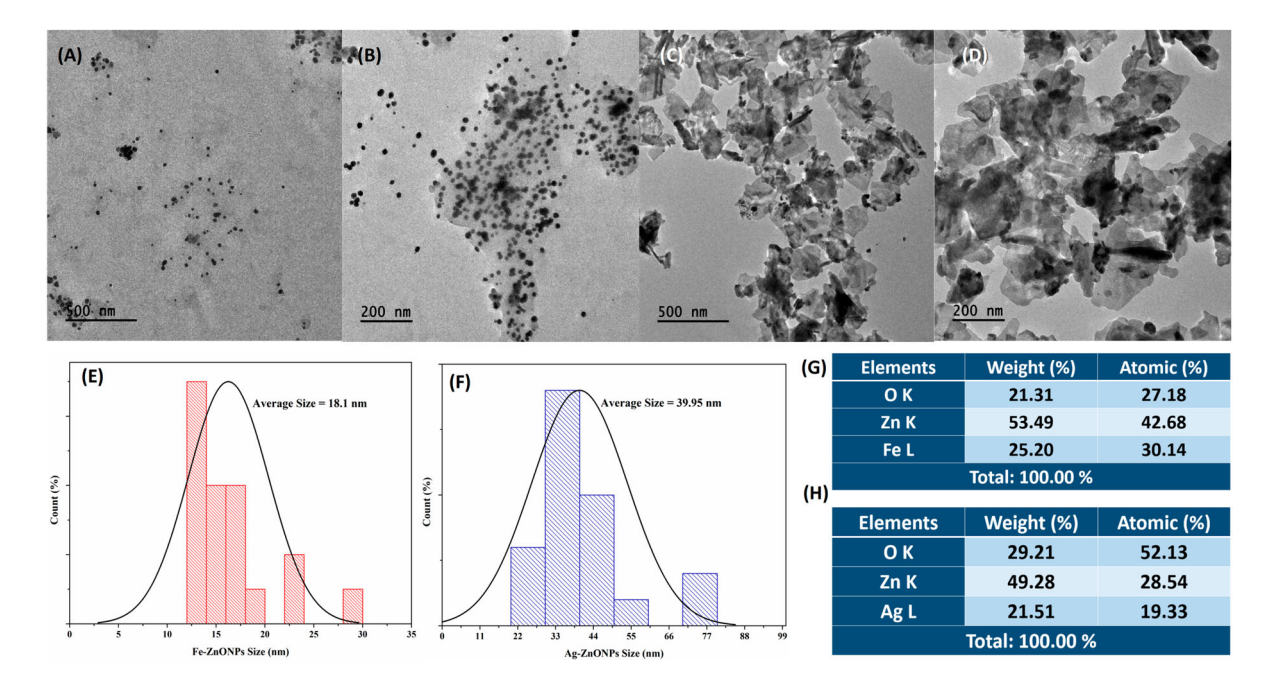


Figure 1. TEM and EDX analysis of BNPs. A. Micrograph of Fe-ZnONPs (500 nm scale); B. Micrograph of Fe-ZnONPs (200 nm scale); C. Micrograph of Ag-ZnONPs (500 nm scale); **D.** Micrograph of Ag-ZnONPs (200 nm scale); **E.** TEM histogram for the size distribution of Fe-ZnONPs; F. TEM histogram for the size distribution of Aq-ZnONPs; G. Elemental Composition of Fe-ZnONPs; H. Elemental Composition of Ag-ZnONPs. (Transmission Electron Microscopy; TEM, Energy Dispersive X-ray; XRD, Bimetallic Nanoparticles; BNPs, Iron-Zinc Oxide Nanoparticles; Fe-ZnONPs, Silver-Zinc Oxide Nanoparticles; Ag-ZnONPs).

molecules. Functional groups (OH, -COOH, -NH₂) from plant metabolites coat BNPs, preventing agglomeration and offering bioactive surfaces. The likely byproducts are acetate and nitrate ions, and oxidized plant compounds [50].

In the case of Fe-ZnONPs, the same Zn-phytoche mical complex is likely formed. Upon the addition of iron sulphate solution, iron ions (Fe²⁺) get partially oxidized to Fe³⁺ in the presence of air and are reduced by plant metabolites to form Fe₃O₄ or Fe₂O₃ particles. These particles integrate into the simultaneously forming ZnO matrix to give Fe-ZnONPs [51]. The functional groups not only act as reducing agents but also prevent the BNPs from agglomerating by coating them. This reaction probably gives the byproducts acetate and sulphate ions and oxidized phytochemicals.

3.3. Characterization of BNPs

3.3.1. TEM and EDX analysis

TEM was employed to study the morphological characteristics of BNPs. According to our findings, Fe-ZnONPs displayed a spherical shape with significant agglomeration (Figure 1A, B). Fe-ZnONPs appeared smaller than Ag-ZnONPs, which exhibited an irregular cubic shape with less agglomeration (Figure 1C, D). In Fe-ZnONPs, agglomeration might be due to the magnetic nature of iron, promoting the clustering of particles. Ansar et al. reported the irregular morphology of Aloe-mediated Ag/ZnONPs heterostructures as well, which aligns with our findings [52]. Similarly, the spherical morphology of Fe-ZnONPs is reported in many research reports [53,54]. The size difference between Ag-ZnONPs and Fe-ZnONPs is consistent with the findings of the literature, where Fe-ZnONPs have often demonstrated smaller diameters due to fast nucleation rates during synthesis. Morphological differences between the two types of BNPs could be attributed to the differences in synthesis conditions, precursor salt ratios, and metal ion reduction rates [55]. Using Image J software, the sizes of BNPs were calculated, and the average sizes of Fe-ZnONPs and Ag-ZnONPs were 18.1 and 39.95 nm, respectively (Figure 1E, F). These sizes coincide with the crystalline sizes calculated using the Debye-Scherrer formula in XRD analysis.

Figure 1 shows the elemental composition of BNPs confirmed by EDX analysis. The Fe-ZnONPs primarily consisted of oxygen (O), zinc (Zn), and iron (Fe), with weight percentages of 21.31%, 53.49%, and 25.20%, respectively (Figure 1G). Similarly, the Ag-ZnONPs primarily consisted of O, Zn, and silver (Ag) with respective weight percentages of 29.21%, 49.28%, and 21.51% (Figure 1H). These results are in line with previous studies, which also report ZnO nanoparticles synthesized with transition metals like Fe and Ag showing similar elemental distributions [4,53,56]. The presence of O and Zn confirms the ZnO matrix, while the metal content (Fe or Ag) demonstrates successful doping.

3.3.2. UV-Vis Spectrophotometry

Surface Plasmon Resonance (SPR) is the characteristic by which the NPs formation and their optical properties are determined. It occurs due to the collective oscillation of free electrons on the metallic NPs surface in

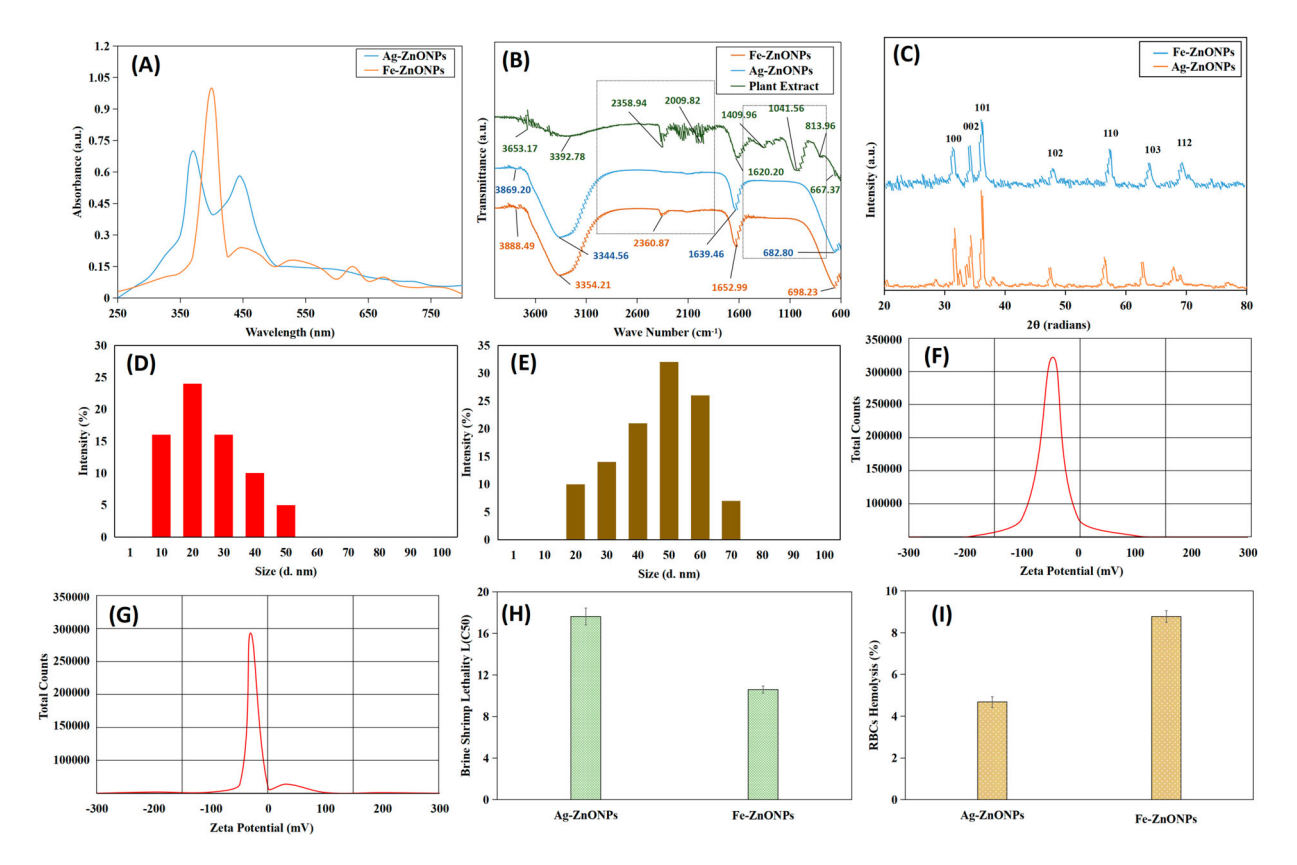


Figure 2. Characterization of Fe-ZnONPs and Ag-ZnONPs. **A.** UV-Vis Spectrum of BNPs; **B.** ATR-FTIR Spectra of nanoparticles relative to Plant Extract (the highlighted regions show the shift in BNPs spectra relative to plant extract); **C.** PXRD Diffractograms of BNPS (JCPDS Card No. 00–036–1451); **D.** Particle Size Distribution of Fe-ZnONPs estimated by DLS Analysis; **E.** Particle Size Distribution of Ag-ZnONPs estimated by DLS Analysis; **F.** Zeta Potential Analysis of Fe-ZnONPs; **G.** Zeta Potential Analysis of Ag-ZnONPs; **H.** BNPs Biocompatibility Analysis using Brine Shrimp Lethality Assay (LC50); **I.** BNPs Biocompatibility Analysis using Red Blood Cells Hemolysis Assay (%). (Iron-Zinc Oxide Nanoparticles; Fe-ZnONPs, Silver-Zinc Oxide Nanoparticles; Ag-ZnONPs, UV-Visible Spectrophotometry; UV-Vis, Bimetallic Nanoparticles; BNPs, Attenuated Total Reflection-Fourier Transform Infrared Spectroscopy; ATR-FTIR, Powdered X-Ray Diffraction; PXRD, Dynamic Light Scattering; DLS).

response to light exposure [57]. This results in the characteristic absorption peaks in the UV-spectrum. In the present study, Ag-ZnONPs exhibited dual peaks at 370 and 446 nm, respectively, corresponding to ZnO and Ag (Figure 2A). The former corresponds to the intrinsic band-gap absorption of ZnO. At the same time, the latter is attributed to the SPR of Ag nanoparticles. In contrast, only a single and distinct peak at 395 nm was observed in the case of Fe-ZnONPs (Figure 2A). This can be explained by the lack of a prominent SPR effect in iron nanoparticles, which typically exhibit weaker or no SPR response in the UV-Vis region due to their dielectric properties. The observed peak may therefore reflect a combined contribution from ZnO and Fe-related transitions. Furthermore, the single peak suggests a more homogeneous and possibly core-shell type structure with uniform distribution, unlike Ag-ZnONPs, where Ag and ZnO exist as distinct domains, reflected in their dual peaks [58]. Our findings coincide with the report published by Devi et al., where Fe-ZnONPs showed a characteristic peak at 370 nm [59]. Likewise, Ehsan et al. observed a broad absorption band with two shoulders in the case of Moringa oleifera-mediated Ag-ZnONPs at 330 nm and 366–79 nm [60]. Comparable findings were reported in the green synthesis of gold nanoparticles (AuNPs) using *Cyperus scariosus* extract, where a single absorption peak at 535 nm indicated successful AuNP formation with uniform characteristics [61]. Thus, the dual peaks of Ag-ZnONPs and the single broad peak of Fe-ZnONPs highlight the significant differences in their optical properties.

3.3.3. ATR-FTIR Spectroscopy

ATR-FTIR Spectroscopy was conducted to identify the functional groups responsible for the stabilization and capping of plant mediated-BNPs, as shown in Figure 2B. For Ag-ZnONPs, prominent peaks appeared at 682.80, 1639.46, 3344.56, and 3869.20 cm $^{-1}$. Similarly, Fe-ZnONPs showed peaks at 698.23, 1652.99, 2360.87, 3354.21, and 3888.49 cm $^{-1}$, while the plant extract exhibited a more complex spectrum with peaks at 667.37, 813.96, 1041.56, 1409.96, 1620.20, 2009.82, 2358.94, 3392.78, and 3653.17 cm $^{-1}$. The peaks in the 1639–1652 cm $^{-1}$ range for both Ag-ZnONPs and Fe-ZnONPs are typically associated with C = O stretching, suggesting the presence of carboxyl groups. The broad peaks observed around 3344–3354 cm $^{-1}$ in both Ag-ZnONPs and Fe-ZnONPs correspond to O-H stretching

Table 1. ATR-FTIR Assignments for Ag-ZnONPs, Fe-ZnONPs, and Plant Extract.

	Wave number (cm ⁻¹)	Functional Groups
Plant Extract		
	667.37	C-H bending (alkyl)
	813.96	C-H out-of-plane bending
	1041.56	C-O stretching (alcohol)
	1409.96	C-H bending (methyl/CH ₂)
	1620.20	C = C stretching (aromatic)
	2009.82	$C \equiv C$ stretching (alkyne)
	2358.94	$C \equiv N$ stretching (nitrile)
	3392.78	O-H stretching (hydroxyl)
	3653.17	O-H stretching (hydroxyl)
Ag-ZnONPs		
•	682.80	C-H bending (alkyl)
	1639.46	C = O stretching (carboxyl)
	3344.56	O-H stretching (hydroxyl)
	3869.20	M-O stretching (metal-oxide bond)
Fe-ZnONPs		-
	698.23	C-H bending (alkyl)
	1652.99	C = O stretching (carboxyl)
	2360.87	C ≡ N stretching (nitrile)
	3354.21	O-H stretching (hydroxyl)
	3888.49	M-O stretching (metal-oxide bond)

vibrations, indicating hydroxyl groups. The broad peaks observed around 3344–3354 cm⁻¹ in both Ag-ZnONPs and Fe-ZnONPs correspond to O-H stretching vibrations, indicating hydroxyl groups. These groups are often associated with the stabilization of NPs as reported in the literature [30, 62,63]. These observations are consistent with findings from the green synthesis of hydroxyethylcellulose phthalate-modified silver nanoparticles, where FTIR spectra revealed similar functional groups contributing to nanoparticle stabilization [64]. A similar study conducted by Jabbar et al. revealed that the bioactive compounds in the Equisetum diffusum extract, used to synthesize Aq-NPs, were most likely coordinated to the metal through carbonyl or hydroxyl groups [65]. Unique peaks near 3869 cm⁻¹ for Ag-ZnONPs and 3888 cm⁻¹ for Fe-ZnONPs confirm the presence of metal-oxide bonds. The plant extract showed additional peaks (e.g. 1409.96 and $3392.78 \, \text{cm}^{-1}$), associated with phenolic and flavonoid compounds, which aid in nanoparticle synthesis. Comparatively, several peaks from the plant extract were absent or shifted in the spectra of Ag-ZnONPs and Fe-ZnONPs, which suggested that these functional groups interacted with the nanoparticles during synthesis, resulting in surface modifications [66]. These results are summarized in Table 1.

3.3.4. PXRD analysis

In the PXRD analysis of BNPs, characteristic peaks were observed at various 2θ angles corresponding to specific reflection planes, and the crystalline nature of the BNPs was consequently confirmed, which has been illustrated in Figure 2C. For Fe-ZnONPs, peaks were observed at 31.72° (100), 34.44° (002), 36.28° (101), 47.52° (102), 56.6° (110), 62.84° (103), and 68.05° (112). Similar peaks were displayed in the case of Ag-ZnONPs at positions 31.75° (100), 34.65° (002), 36.25°

(101), 47.55° (102), 56.55° (110), 62.85° (103), and 67.95° (112). This suggested a comparable crystal structure for both nanoparticle types. The diffraction pattern aligns closely with the wurtzite hexagonal phase typically associated with ZnO-based NPs (JCPDS Card No. 00–036–1451). The slight differences in peak positions may be due to the incorporation of Ag and Fe, potentially causing minor lattice distortions. The narrow and sharp peaks, especially in Ag-ZnONPs, indicate a highly crystalline nature. The crystalline size of BNPs was found using PXRD data and Debye-Scherrer's formula $(d = K\lambda/\beta\cos\theta)$. It was found to be ~ 42.4 nm for Ag-ZnONPs and ~ 18.88 nm for Fe-ZnONPs. These values align well with the TEM images, which reveal that Fe-ZnONPs are smaller and have a more spherical shape compared to the larger, irregular cubic shape observed in Ag-ZnONPs. The consistent size and shape observations across both XRD and TEM confirm the crystalline nature and morphology of the nanoparticles and underscore the reliability of the results. Our findings corroborate with the study by Hussain et al. and Raza et al., who observed a similar crystalline structure for Aq-ZnONPs [67,68]. For Fe-ZnONPs, the results reported by Gudla et al. and Wenjuan et al. showed that the spherical shape of Fe-ZnONPs is common [69,70]. These findings confirm the successful doping of the ZnO matrix with Ag and Fe, which may influence the NPs' physical and catalytic properties.

3.3.5. DLS and zeta potential investigations

DLS analysis revealed that the particle size distribution of Fe-ZnONPs was within the 10-50 nm range (Figure 2D), while Aq-ZnONPs showed a broader size distribution of 20-70 nm (Figure 2E). The smaller size range of Fe-ZnONPs corroborates well with the previously obtained TEM data, which also indicated Fe-ZnONPs to be smaller in size compared to Ag-ZnONPs. This size difference may be attributed to the inherent material properties and synthesis conditions for each nanoparticle type. Narendhran et al. reported the particle size of 22-44 nm for Fe-ZnONPs, which coincides with our results [71]. Comparable results were reported by Mohammadi-Aghdam et al., where a 60-90 nm size was observed for Ag-ZnONPs [72].

The zeta potential values provide insight into the stability of the nanoparticles. In this study, Fe-ZnONPs exhibited a zeta potential of -45.2 mV (Figure 2F), while Ag-ZnONPs had a slightly lower value of -31.2 mV (Figure 2G). The high negative zeta potential values of BNPs were attributed to the negative charge of the phytochemicals of M. asiatica extract, likely due to the presence of negatively charged functional groups such as hydroxyl (-OH) and carboxyl (-COO⁻) on the BNPs surfaces. This demonstrates the presence of plant phytochemicals on the surface of BNPs. The findings indicate that both BNPs were stable, as reported in the literature by Abdul Hassan et al [73]. However, Ag-ZnONPs

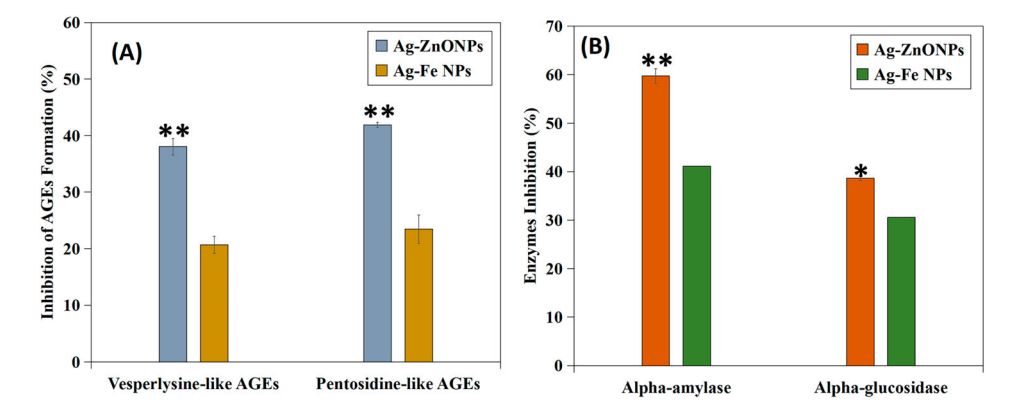


Figure 3. A. Anti-glycation Investigation in terms of vesperlysine-like and pentosidine-like Advanced Glycation End Products (AGEs) inhibition; B. Anti-diabetic Investigation in terms of alpha-amylase and alpha-glucosidase inhibition; Each column represents mean \pm SD and * represents a significant difference between Ag-ZnONPs and Fe-ZnONPs treatment (p < 0.05).

had less stability as compared to Fe-ZnONPs, showing a slight degree of agglomeration. These stability values are consistent, as zeta potentials closer to zero indicate a higher likelihood of agglomeration, while more negative values promote repulsion and thus stability [74]. Consequently, Fe-ZnONPs are less prone to agglomeration in colloidal systems, making them more stable than Ag-ZnONPs, which are relatively more likely to aggregate under similar conditions.

3.4. Biocompatibility of BNPs

Biocompatibility of BNPs was determined using the Brine Shrimp Lethality (BSL) Assay and the RBC Hemolysis assay. In the BSL assay, our findings, as shown in Figure 2H, presented that Ag-ZnONPs exhibited an LC50 of 17.62 ± 0.81 mg/mL, classifying them as moderately toxic. As compared to them, Fe-ZnONPs had a lower LC50 value (9.5 \pm 0.34 mg/mL). According to the toxicity classification, substances that have LC-50 values between 10.0-30 mg/mL are moderately toxic, and those between 1.0–1.0 mg/mL are considered toxic. Based on these values, Ag-ZnONPs are comparatively less toxic than Fe-ZnONPs. This suggests that even though both BNPs have some degree of toxicity, Fe-ZnONPs pose a higher toxicological risk as compared to Ag-ZnONPs. This may be attributed to the high oxidative potential of Fe. However, both BNPs demonstrated safe profiles regarding hemolysis as observed in Figure 2I. Ag-ZnONPs exhibited $4.68 \pm 0.26\%$ and Fe-ZnONPs showed $4.90 \pm 0.28\%$ of hemolysis, both remaining within the acceptable range of \leq 5%, as set by the American Society for Testing and Materials, indicating good biocompatibility for both types of BNPs [75]. When comparing these results with the existing literature, it was evident that Fe-ZnONPs may pose a higher cytotoxicity risk, aligning with the study by Xu et al. that reported Fe-based nanoparticles to exhibit moderate toxicity at lower concentrations due to their oxidative potential [76]. Ag-ZnONPs, on the other hand, have been consistently shown to have lower cytotoxic effects, which supports their safer biocompatibility profiles [77,78].

3.5. Antiglycation activity of BNPs

Antiglycation property of NPs refers to their ability to inhibit AGEs formation, as they are linked to aging and chronic disorders. BNPs such as Ag-ZnONPs and Fe-ZnONPs are reported to show potent antiglycation effects as they scavenge ROS species and avoid the glycation of proteins in the cells [4]. Therefore, they offer potential therapeutic benefits in managing conditions associated with glycation damage. In our study, the inhibition of V-AGEs and P-AGEs was observed (Figure 3A). Ag-ZnONPs exhibited $38.0 \pm 1.5\%$ inhibition against V-AGEs and 41.9 \pm 0.5% inhibition against P-AGEs. However, in the case of Fe-ZnOPs, less inhibition (20.7 \pm 1.5% against V-AGEs and 23.5 \pm 2.5% against P-AGEs) was observed as compared to Ag-ZnONPs. The superior anti-glycation potential of Ag-ZnONPs has been established in previous literature reports [4,29,46]. Badhusha et al. reported that Fe-ZnONPs have the anti-glycation ability as they were found to interact with Bovine Serum Albumin (BSA) protein and quench its fluorescence [79]. It has been reported that the enzyme-BNPs interaction depends on the size and shape of the BNPs [80]. The higher values for Ag-ZnONPs in our study can be attributed to the smaller size and spherical morphology as compared to irregular cubic Fe-ZnONPs.

3.5.1. Antiglycation mechanism of BNPs

BNPs prevent the glycation of proteins through a combination of surface interactions with proteins, free radical scavenging, disruption of sugar-protein binding, and inhibition of crosslink formation. The schematic representation is shown in Figure 4.

The high surface area-to-volume ratio of BNPs allows them to interact extensively with proteins [81]. This interaction can lead to the blocking of glycation sites, such as free amino groups on proteins, which prevents

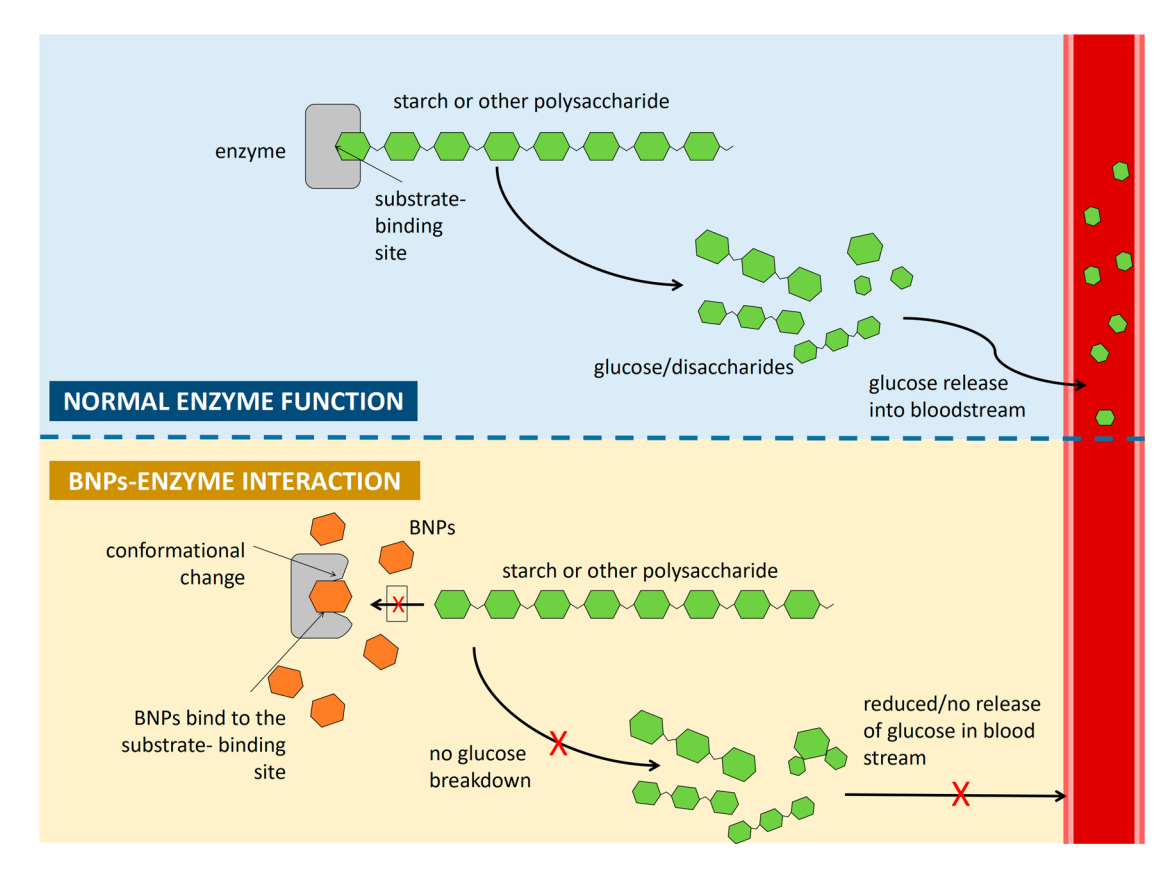


Figure 4. Probable Mechanism of Antidiabetic Enzyme Inhibition by Bimetallic Nanoparticles (BNPs). **Top:** Normal enzyme function showing glucose release from polysaccharide digestion. **Bottom:** BNPs binding inhibits substrate breakdown, preventing glucose release

sugars from binding with proteins. As a result, the formation of Amadori Products, which are early glycation intermediates, is halted [82]. BNPs can also form electrostatic or covalent bonds with functional groups in protein, which further inhibit the production of AGEs [83]. Another mechanism is the disruption of sugarprotein binding. BNPs compete with the sugars for protein binding sites and obstruct their reactions with protein amino groups. By effectively binding these sites, NPs prevent the production of glycation intermediates and subsequently, AGEs. Moreover, they can also block the glycation-induced crosslinking of proteins by breaking the existing crosslinks or preventing their formation in the first place. Some NPs alter the conformation of proteins and prevent structural changes required for cross-linking [84].

Yet another pathway for antiglycation activity is the radical scavenging and metal ions chelation as oxidative stress promotes glycation. BNPs that have inherent antioxidant properties scavenge free radicals and reduce oxidative damage, thereby preventing the promotion of glycation reactions. Moreover, BNPs that have metal-ion chelating properties reduce the availability of ions that catalyze oxidation reactions and promote glycation. The reduction of these ions results in the lowering of oxidative stress and subsequent glycation [85]. The ability of nanoparticles to act as both physical blockers and chemical antioxidants has made them

effective antiglycation agents in numerous biomedical applications.

3.6. Antidiabetic activity of BNPs

To evaluate the potential of NPs to inhibit the activity of enzyme competitively contributing in diabetes, α glucosidase and α -amylase inhibition assays were conducted. Figure 3B shows the results that were reported as a percentage of inhibition. For Ag-ZnONPs, the analysis showed a promising value of $38.60 \pm 0.26\%$ and 59.70 \pm 1.32% respectively. Regarding Fe-ZnONPs, $30.60 \pm 2.07\%$ inhibition and $41.13 \pm 1.58\%$ inhibition were observed against α -glucosidase and α -amylase, respectively. Anjum et al. reported that Aq-ZnO BNPs led to the highest inhibition of α -glucosidase (41.6 \pm 1.00%) and α -amylase (59.7 \pm 1.01%) as compared to their monometallic counterparts [4]. Our literature search did not find any reports regarding the antidiabetic analysis of Fe-ZnONPs in terms of inhibition against key diabetic enzymes. This is the first study of its kind that showed that Fe-ZnONPs have a high ability to suppress α -amylase and α -glucosidase activity and demonstrate strong anti-diabetic properties.

3.6.1. Mechanism of antidiabetic action of BNPs

Diabetes mellitus is marked by high blood glucose levels due to insufficient insulin or poor cellular response

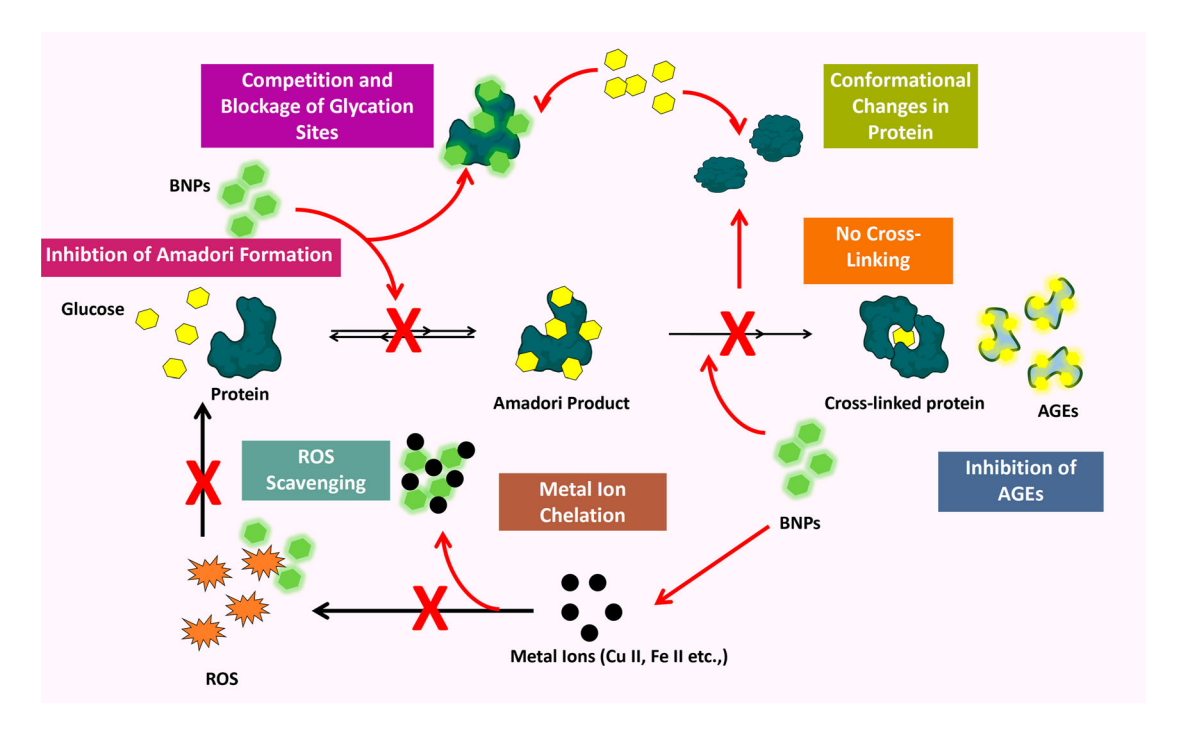


Figure 5. Schematic Representation of the Antiglycation Mechanisms of BNPs. Black Arrows: Normal Process of AGEs Formation; Red Arrows: BNP-mediated inhibition through competition at glycation sites, ROS scavenging, metal ion chelation, and prevention of protein cross-linking. (Bimetallic Nanoparticles; BNPs, Advanced Glycation End Products; AGEs, Reactive Oxygen Species; ROS).

to it. Under prolonged conditions, it can even lead to neurological disorders, including conditions like carpal tunnel syndrome and Bell's palsy [86]. It is crucial to control postprandial glucose levels, as enzymes like α amylase and α -glucosidase break down carbohydrates into sugars [87]. BNPs have shown promise as alternative inhibitors of these enzymes, offering a novel approach to glycemic control with fewer side effects than traditional treatments [88]. Figure 5 shows the probable mechanism of diabetic enzymes inhibition in cells. BNPs may form electrostatic interactions with functional groups (such as amino or carboxyl groups) present in enzymes. This interaction can alter the enzyme's charge distribution or interfere with the binding of the substrate, inhibiting the enzyme's function [89]. BNPs can bind to the active sites of enzymes, the region where the substrate (such as starch or disaccharides) would normally bind. By blocking the active site, BNPs prevent the enzyme from interacting with its substrate, reducing the breakdown of complex carbohydrates into simple sugars like glucose [90]. This slows the release of glucose into the bloodstream, which helps manage blood sugar levels. Furthermore, as in antiglycation, BNPs might effectively compete with the substrate for enzyme binding, especially at glycation sites, where sugars typically bind [7]. Our study reported that both Ag-ZnONPs and Fe-ZnONPs possess high antidiabetic potential in terms of enzyme inhibition.

3.7. Antioxidant analysis of BNPs

Oxidative stress is caused by an imbalance between antioxidants and free radicals in the body. It is linked

to the progression of various diseases such as cancer, diabetes, and neurodegenerative disorders. In this study, a series of cell-free assays, including ABTS, ORAC, CUPRAC, and FRAP, were used to evaluate the antioxidant activity of the synthesized BNPs to comprehensively assess their radical scavenging and reducing capacities as demonstrated in Figure 6. In the case of Ag-ZnONPs, the ABTS assay demonstrated a favourable scavenging activity, with a radical inhibition of 34.0 \pm 0.8 μM TEAC (Figure 6A). Similarly, the ORAC assay, which measures peroxyl radical scavenging activity, revealed a high antioxidant capacity of 16.4 ± 1.3 μΜ TEAC (Figure 6B). The CUPRAC assay, which evaluates the cupric ion reducing power, recorded a value of 205.9 \pm 16.2 μ M TEAC, indicating the strong reducing potential of the Ag-ZnONPs (Figure 6C). Finally, the FRAP assay showed a ferric reducing power of $161.9 \pm 9.3 \,\mu\text{M}$ TEAC, consistent with the CUPRAC assay, confirming that our Ag-ZnONPs work effectively by electron transfer (ET) mechanism (Figure 6D). In comparison, Fe-ZnONPs showed the highest anti-oxidative potential of 106.6 \pm 4.2 μM TEAC when assessed via CUPRAC assay, followed by FRAP (70.2 \pm 0.4 μ M TEAC), ABTS (18.7 \pm 1.5 μ M TEAC), and ORAC (8.5 \pm 0.3 μ M TEAC). Fe-ZnONPs also showed efficacy via the ET mechanism, but they were found to have less anti-oxidative power when compared to Ag-ZnONPs. The most probable explanation can be the metal combination in Ag-ZnO, which results in better synergy between the silver and zinc, further amplifying their combined antioxidant activity. In contrast, iron's relatively lower redox potential than silver may reduce its ability to scavenge free radicals as efficiently. This is supported by the study

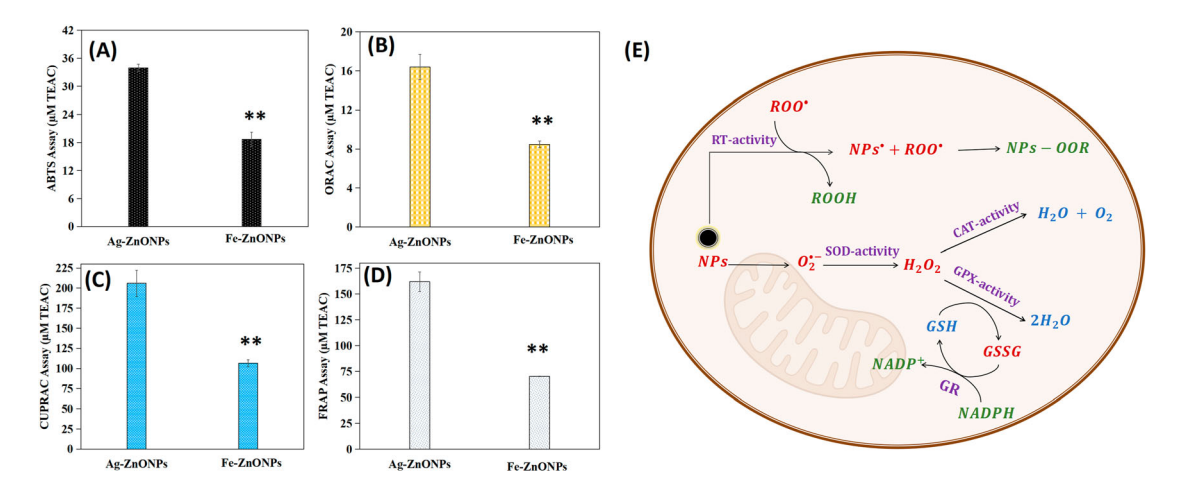


Figure 6. Antioxidant Activity of BNPs. **A.** ABTS Assay; **B.** ORAC Assay; **C.** FRAP Assay; **D.** CUPRAC Assay; **E.** Possible Mechanism of Antioxidant Action of BNPs in Cells by RT, SOD, CAT, GPX and GR mimetic activity (Bimetallic nanoparticles, BNPs; 2,2-Azinobis-3-ethylbenzthiazoline-6-sulphonic acid, ABTS; Oxygen Radical Absorbance Capacity, ORAC; Ferric Reducing Antioxidant Power, FRAP; Cupric Reducing Antioxidant Capacity, CUPRAC, radical-trapping, RT; glutathione, GSH; Glutathione peroxidase, GPX; Superoxide Dismutase, SOD; Catalase, CAT; Glutathione Disulfide, GSSH). Each column represents mean \pm SD and * represents the significant difference between Ag-ZnONPs and Fe-ZnONPs treatment (p < 0.05).

conducted by Shejawal et al., where the antioxidant ability of the metallic counterparts was studied, and AgNPs were found to have higher ROS-scavenging potential than FeNPs [91].

3.7.1. Probable antioxidant mechanism of BNPs in cells

Nanomaterials possess inherent antioxidant properties due to their surface characteristics, independent of their functionalization. There are two essential mechanistic pathways by which nanoparticles defend against oxidative stress, i.e. chain-breaking antioxidant pathway, also known as the radical trapping (RT) pathway, and enzyme mimetic preventive oxidant pathway. However, these mechanisms work by the fundamental principle, i.e. reduction-oxidation (redox) reactions [92,93]. The pathways are summarized in Figure 6E. In the chain-breaking/RT antioxidant pathway, direct interaction between the NPs and the free radicals (reactive oxygen species, ROS) and NPs neutralize them by donating electrons to the free radicals similar to how the traditional antioxidants act [94]. For instance, NPs can quench alkyl peroxyl radicals (ROO*) and transform them into neutral hydroperoxides (ROOH) [95]. The other mechanism is the enzyme-mimetic pathway in which NPS mimic the activity of antioxidant enzymes present in the cells such as CAT, Glutathione peroxidase (GPX), and SOD [96]. CAT-mimetic NPs can decompose hydrogen peroxide H₂O₂ into water and oxygen at neutral and basic pH levels. This activity is influenced by the oxidation state of nanoparticles [97]. High surface ionic ratios enhance the CAT-like antioxidant activity of nanoparticles [98]. GPX-mimetic NPs reduce H₂O₂ to water using glutathione (GSH) by forming polar peroxido- species rather than hydroxyl radicals, which facilitates the reduction of H₂O₂ with GSH [99]. This behaviour has been studied in a few types of nanomaterials as compared to the CAT-like mechanism of antioxidation [100]. In the case of superoxide radical decomposition, the self-decay of superoxide is pH-dependent, with maximum efficiency at acidic pH and reduced efficiency at physiological pH [101]. Given the slow self-decay of superoxide at physiological pH, the enzyme SOD evolved naturally to accelerate this process [102]. SOD-mimetic NPs efficiently catalyze the reduction of superoxide to hydrogen peroxide and oxygen. Various nanomaterials have demonstrated high SOD-like activity and have the potential for applications where rapid superoxide quenching is needed [103].

3.8. Anticancer activity of BNPs

3.8.1. Cell viability analysis

HepG2 cell cultures were used to determine the anticancer effect of BNPs. Our findings demonstrated that Ag-ZnONPs reduced the cell viability to $48.5 \pm 2.3\%$ compared to NTCs, whereas Fe-ZnONPs showed $28.5 \pm 1.4\%$ which is far lesser than Ag-ZnONPs (Figure 7A). This indicates the superior toxic effect of Fe-ZnONPs. Carofiglio *et al.* reported similar findings where Fe-ZnONPs were found extremely cytotoxic even at low concentrations as compared to their monometallic counterpart [104]. In contrast, 20% viability was observed in another report when Burkitt's lymphoma Daudi cell lines were treated with Fe-ZnONPs which supports to our findings [53]. The greater cytotoxicity of Fe-ZnONPs in our study may be attributed to their smaller size and enhanced cellular uptake.

3.8.2. Disruption of mitochondrial membrane potential

An important parameter to understand the anticancer activity of any therapeutic agent is to determine the mitochondrial potential of the cancerous cells. The loss



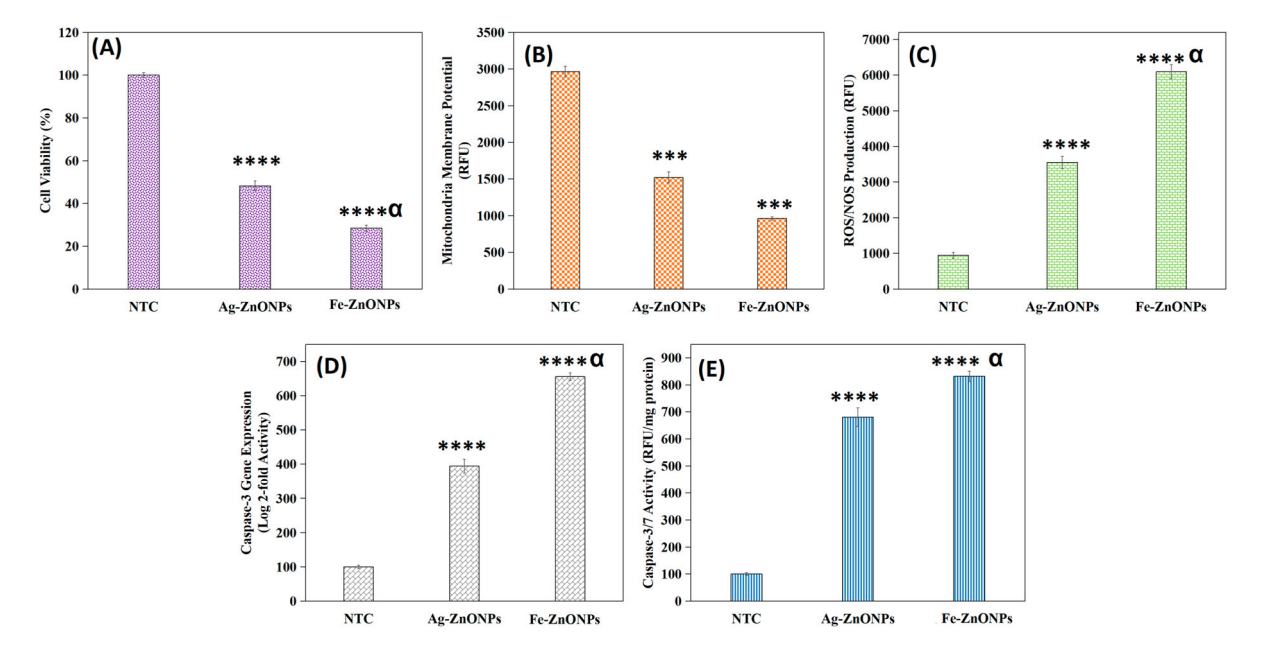


Figure 7. Anticancer Evaluation of Aq-ZnONPs and Fe-ZnONPs-treated HepG2 cells relative to non-treated cells (NTCs). A. Cell Viability (%); **B.** Mitochondrial Membrane Potential (RFU); **C.** ROS/NOS Production (RFU); **D.** Caspase-3 Gene Expression (Log 2-fold Activity); **E.** Caspase-3/7 Expression (RFU/mg protein). Each column represents mean \pm SD, * represents a significant difference between NTCs and BNPs-treated cells and α represents a significant difference between Ag-ZnONPs treatment and Fe-ZnONPs treatment (p < 0.05).

of MMP depicts the disruption of the electron transport chain (ETC) in mitochondria subsequently leading to ATP depletion and cell death [105]. In the present study, Aq-ZnONPs caused a 2-fold decrease in the MMP (1521.67 \pm 74.19 RFU) as compared to NTCs $(2965 \pm 74.54 \, \text{RFU})$, which indicated that mitochondrial function was significantly disrupted (Figure 7B). This is supported by Anjum *et al.* where MMP of 1796.3 \pm 61.09 RFU was reported [4]. However, Fe-ZnONPs showed the highest reduction in MMP with 962 \pm 22.53 RFU. This is in line with the results of our other parameters establishing that Fe-ZnONPs are superior anticancer agents as opposed to Aq-ZnONPs. The stronger impact of Fe-ZnONPs on MMP could be attributed to their capacity to interact with the mitochondrial membrane more effectively. This interaction leads to the enhanced permeability and disruption of ETC as discussed by Ragab et al [106].

3.8.3. ROS/NOS production

Ag-ZnONPs treatment resulted in the 3553.67 \pm 169.77 RFU of ROS/NOS levels which is four times greater than that of NTCs. However, Fe-ZnONPs showed the greatest production of ROS/NOS with 6094.00 ± 197.58 RFU (Figure 7C). The high production of oxidative species is associated with an increased rate of cellular damage and apoptosis ultimately resulting in the cell death [107]. Opposingly, it was previously reported in the literature, that iron reduces the ability of Zn⁺² ions to dissolve in the cytoplasm resulting in decreased oxidative stress [108]. However, recent studies suggest that iron can initiate cellular death in the process called ferroptosis, which is an iron-dependent accumulation of lipid reactive oxygen species (ROS) and remnant Zn + 2 ions accelerate this process [109]. Therefore, it can be proposed that our Fe-ZnONPs might result in higher ROS/NOS production via ferroptosis.

3.8.4. Upregulated caspase-3 gene expression and enhanced caspase-3/7 activity

The most widely reported mechanism of anticancer action is apoptosis and caspase family proteins are the key contributors to initiating and carrying out the programmed cell death. The current study findings corroborate with the already published literature reports. Our Ag-ZnONPs upregulated the caspase-3gene expression with 394.11 \pm 20.21 log 2-fold activity, while Fe-ZnONPs induced a 2-fold increase with 655.55 \pm 11.13 log 2-fold activity (Figure 7D).

Furthermore, caspase 3/7 activity was enhanced the most by Fe-ZnONPs treatment 831.79 ± 19.21 RFU/mg protein, as compared to Ag-ZnONPs where 680.43 ± 34.89 RFU/mg protein activity was observed (Figure 7E). Both types of BNPs showed high caspase 3/7 activity as compared to NTCs, however, Fe-ZnONPs were found to be most inducing. Many studies have shown the significant potential of BNPs to directly influence caspase activity and activate apoptosis in cancer cells and our findings corroborate with them [56,110]. This enhanced activation of the apoptotic pathway by Fe-ZnONPs could be due to enhanced oxidative stress levels which directly influence caspase expression and activate the apoptotic cascade as explained by Zheng et al [111].

3.8.5. Potential anticancer mechanism of BNPs

Several pathways by which the nanomaterials induce tumour death have been reported. These pathways can

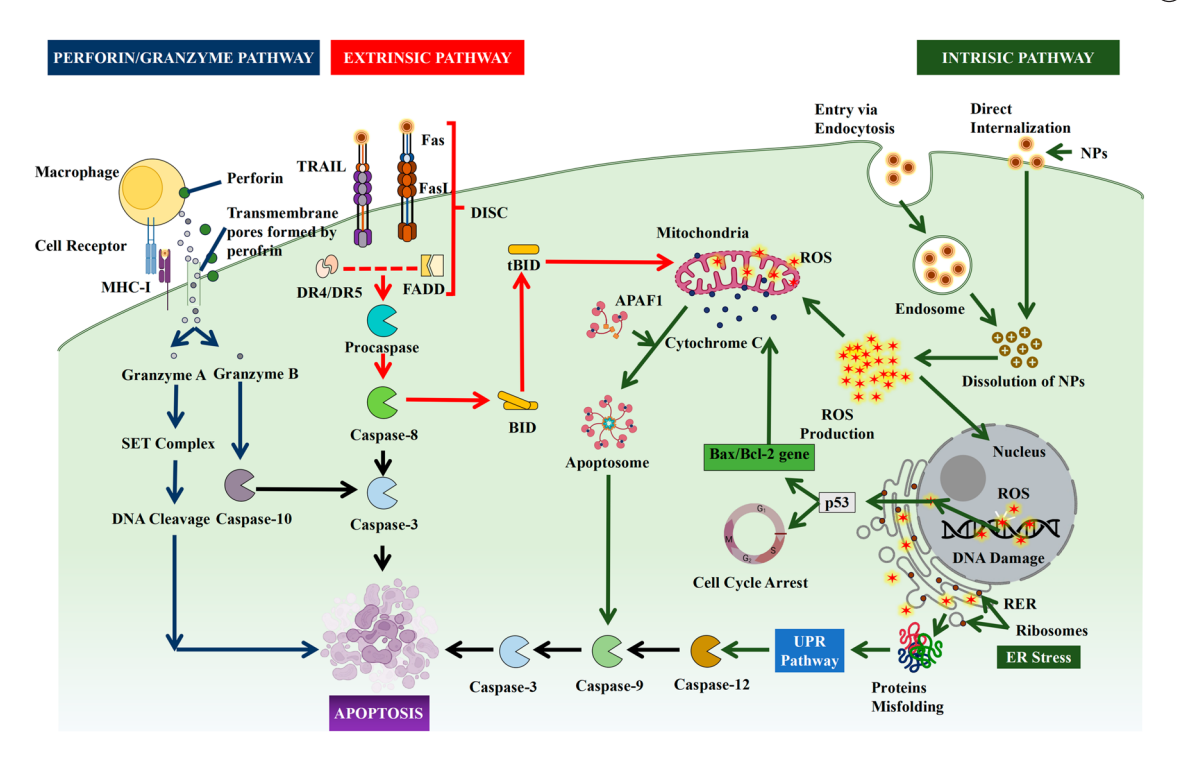


Figure 8. Proposed illustration of the anticancer mechanisms of nanoparticles, highlighting the Perforin/Granzyme (**blue arrows**), Extrinsic (**red arrows**), and Intrinsic pathways (**green arrows**) through various cellular processes including ROS production, mitochondrial damage, DNA cleavage, and protein misfolding resulting in the apoptosis via Caspase Pathway (**black arrows**). [Nanoparticles, NPs; reactive oxygen species, ROS; Rough Endoplasmic Reticulum, RER; Endoplasmic Reticulum, ER; Major Histocompatibility Complex, MHC; Tumor Necrosis Factor (TNF)-related apoptosis-inducing ligand, TRAIL; Fas-associated death domain, FADD; Fas ligand, FasL; death-inducing signalling complex, DISC; Truncated BID, tBID].

be divided into three categories i.e. intrinsic pathways, extrinsic pathways, and perforin/granzyme pathways (Figure 8).

In intrinsic pathways, NPs enter the cell and dissolve due to a low pH environment resulting in dyshomeostasis, which further induces the production of ROS in the cytoplasm [112]. The accumulation of ROS leads to oxidative stress, which not only causes DNA damage but can also damage various organelles and affect the physiology of cellular components. Prolonged oxidative damage can initiate the p53-Bax/Bcl-2 pathway of apoptosis, causing the upregulation of p53 gene, which can result in the G1- and S-phase cell arrest. p53 also upregulates Bax/Bcl-2 gene, leading to the loss of mitochondrial function by disrupting mitochondrial membrane potential (MMP) [113]. Consequently, the release of pro-apoptotic factors such as cytochrome C from the mitochondrial intermembrane space occurs, beginning the caspase pathway of apoptosis [114]. Additionally, the accumulation of metal ions in the cytoplasm can cause endoplasmic reticulum (ER) stress, resulting in protein misfolding in the ER lumen. It activates the unfolded protein response (UPR) pathway and initiates apoptosis [31].

NPs extrinsically induce apoptosis by activating Tumor Necrosis Factor (TNF)-related apoptosis-inducing ligand (TRAIL)-dependent pathway and Fas/FasL pathway [115,116]. In Fas/Fasl pathway, external stimuli (i.e. NPs) interact with the Fas receptor, which then binds

with Fas ligand (FasL) to form a complex and recruits Fas-associated death domain (FADD) adapter protein, resulting in the formation of the death-inducing signalling complex (DISC) [117]. In the TRAIL pathway, death receptors, DR4/DR5 play a significant role in activating the apoptotic cascade. External stimuli, namely NPs, result in the activation and binding of death receptors with TRAIL. TRAIL-dependent and Fas/FasL machinery work in coordination, as the binding of DR4 and DR5 with TRAIL leads to conformational changes in death receptors (DRs). These changes promote interaction with FADD. Once DISC binds with DR4/DR5, it recruits procaspases, which, upon proteolysis, are activated to form caspase-8, further leading to the formation of apoptosis execution machinery including, downstream effector caspases [118]. Moreover, caspase-8 cleaves the pro-apoptotic protein Bid and converts it into its active truncated form (tBid). tBid then translocates to the mitochondria and initiates the intrinsic apoptotic process.

In the perforin/granzyme pathway of programmed cell death, nanoparticles enhance the function and formation of phagocytic cells, such as macrophages, which secrete perforin. Perforin forms transmembrane pores in tumour cells, and allows exophytic release of cytoplasmic granules, rich in proteases like granzyme A and B, to enter. Granzyme A recruits the DNA digesting enzymes complex known as SET complex and results in DNA cleavage leading to cell death. Granzyme B induces



apoptosis by activating caspase-10 and downstream effectors in the caspase pathway [119].

4. Conclusions

Overall, this study elucidates the therapeutic potential of *M. asiatica*-mediated BNPs, specifically Ag-ZnONPs and Fe-ZnONPs, in the context of antioxidant, anticancer and anti-diabetic applications. Both types of nanoparticles exhibited significant anticancer properties, with Fe-ZnONPs demonstrating a ROS/NOS production level of 6094.00 ± 197.58 RFU and Ag-ZnONPs with a value of 3553.67 + 169.77 RFU, however, Fe-ZnONPs displayed superior efficacy despite their lower biocompatibility compared to Ag-ZnONPs. These findings underscore the unique profile of Fe-ZnONPs as promising candidates for targeted cancer therapies. Moreover, Ag-ZnONPs proved to be better antiglycation agents with a P-AGEs inhibition percentage of $41.9 \pm 0.5\%$ as compared to Fe-ZnONPs that only displayed a value of 23.5 \pm 2.5%. Furthermore, in terms of anti-diabetic potential, Ag-ZnONPs were identified as the superior BNPs again with an α -amylase inhibition potential of 59.70 \pm 1.32% in comparison with the $41.13 \pm 1.58\%$ of Fe-ZnONPs. Lastly, Ag-ZnONPs also demonstrated the greater efficacy as an anti-oxidant with 161.9 \pm 9.3 μM TEAC in the FRAP assay relative to $70.2 \pm 0.4 \,\mu\text{M}$ TEAC of Fe-ZnONPs.

The significance of this study lies in the comparative analysis of Ag-ZnONPs and Fe-ZnONPs and highlights the former's safer biocompatibility and enhanced therapeutic effects. This distinction is particularly important for the development of novel therapeutic strategies and emphasizes the need for a balanced approach that weighs therapeutic efficacy against potential biocompatibility issues. Furthermore, our results align with and expand upon the existing literature by providing new insights into the applications of Fe-ZnONPs, which have not been extensively studied prior to this research. This positions our findings as a valuable contribution to the field and pave the way for further exploration into the mechanisms of action and potential applications of BNPs in biomedical contexts at a larger, commercial level.

Notably, the M. asiatica Leaf Extract used in the synthesis played a crucial role as both a reducing and stabilizing agent, likely contributing phytochemicals that enhanced the biological activity of the nanoparticles. While a direct comparison of the leaf extract alone versus the BNPs was not within the scope of this study, its known therapeutic potential warrants further investigation to isolate and evaluate its individual biological effects. Future work could explore this comparison to better understand the synergistic or additive roles of the extract in nanoparticle-mediated therapies.

Moreover, this study acknowledges certain limitations, including the need for more comprehensive assessments of long-term biocompatibility and nanotoxicity. It is imperative to focus future research on invivo studies to evaluate the biological impacts of BNPs in more complex physiological environments, along with the investigations into dose-response relationships to establish therapeutic windows and identify potential toxicity thresholds.

Acknowledgement

The authors extend their appreciation to Taif University, Saudi Arabia, for supporting this work through project number (TU-DSPP-2024-74). Moreover, we thank Kinnaird College for Women University for providing space and resources required for this study.

Authors contribution

Conceptualization: S.A., F.A and M.I.; Methodology: S.A., M.I., Z.H, C.H., and I.A.; Project Administration: S.A., S.B.A., M.M.S.; Formal Analysis, Software and Validation: S.A., M.I., A.Y.J., C.H.; Writing – Original Draft: M.I., I.A., K.S.A., Z.H., and A.Y.J.; Writing – Review & Editing: S.A., M.M.S., and C.H; Funding: S.A, F.A., and M.M.S., Supervision: S.A and C.H.

Disclosure statement

No potential conflict of interest was reported by the author(s).

Funding

This research was funded by Taif University, Saudi Arabia, Project Number (TU-DSPP-2024-74).

Ethical consideration

This experiment was performed in consideration with the ethical standards of the International and National Research Committees as well as 1964 Helsinki Declaration and its later amendments due to the involvement of human participants.

Ethical approval

Ethical approval (KCRC: 122) was taken from the Ethical review committee of Kinnaird College for Women University, Lahore, Pakistan.

Consent

Consent was obtained from the participants.

Data availability statement

All the data of the study are incorporated in the published manuscript.

ORCID

Mubashra Inam http://orcid.org/0009-0002-1138-6781 Fayez Althobaiti http://orcid.org/0000-0002-8344-9238 Mohamed Mohamed Soliman http://orcid.org/0000-0001-7208-7123

Khalid S. Alotaibi http://orcid.org/0009-0000-1333-4446 Shatha B. Albattal http://orcid.org/0009-0009-4919-6300

References

- [1] Belenov SV, Volochaev VA, Pryadchenko VV, et al. Phase behavior of Pt-Cu nanoparticles with different architecture upon their thermal treatment. Nanotechnol Russ. 2017;12(3):147-155. doi:10.1134/S1995078017020033
- [2] Arora N, Thangavelu K, Karanikolos GN. Bimetallic nanoparticles for antimicrobial applications. Front Chem. 2020;8:412. doi:10.3389/fchem.2020.00412
- [3] Sharma G, Kumar A, Sharma S, et al. Novel development of nanoparticles to bimetallic nanoparticles and their composites: a review. J King Saud Univ - Sci. 2019;31(2):257-269. doi:10.1016/j.jksus.2017.06.012
- [4] Anjum S, Nawaz K, Ahmad B, et al. Green synthesis of biocompatible core-shell (Au-Ag) and hybrid (Au-ZnO and Ag-ZnO) bimetallic nanoparticles and evaluation of their potential antibacterial, antidiabetic, antiglycation and anticancer activities. RSC Adv. 2022;12(37):23845-23859. doi:10.1039/D2RA03196E
- [5] Jana TK, Jana SK, Kumar A, et al. The antibacterial and anticancer properties of zinc oxide coated iron oxide nanotextured composites. Colloids Surf B. 2019;177:512-519. doi:10.1016/j.colsurfb.2019.02.041
- [6] Turabik M, Özdemir S, Akinbingol G, et al. Comparison of antioxidant, antimicrobial, DNA cleavage, cell viability, and biofilm inhibition activities of mono- and bimetallic copper and zinc nanoparticles. Inorg Chem Commun. 2023;155:111072. doi:10.1016/j.inoche.2023.111072
- [7] Nyabadza A, McCarthy É, Makhesana M, et al. A review of physical, chemical and biological synthesis methods of bimetallic nanoparticles and applications in sensing, water treatment, biomedicine, catalysis and hydrogen storage. Adv Colloid Interface Sci. 2023;321:103010. doi:10.1016/j.cis.2023.103010
- [8] Bashir I, et al. Antioxidant and anticancer silver nanoparticles of Mentha asiatica aerial part extract: a novel study. Inorg Nano-Metal Chem. 2021;54:1-7.
- [9] Mikaili P, Mojaverrostami S, Moloudizargari M, et al. Pharmacological and therapeutic effects of Mentha Longifolia L. and its main constituent, menthol. Anc Sci Life. 2013;33(2):131-138. doi:10.4103/0257-7941. 139059
- [10] Ying S, Guan Z, Ofoegbu PC, et al. Green synthesis of nanoparticles: current developments and limitations. Environ Technol Innov. 2022;26:102336. doi:10.1016/j. eti.2022.102336
- [11] Khosravi K, et al. Green synthesis of metallic nanoparticles using algae and microalgae. Lett Appl NanoBioSci. 2019;8:666-670. doi:10.33263/LIANBS83.666670
- [12] Ullah S, Khalid R, Rehman MF, et al. Biosynthesis of phyto-functionalized silver nanoparticles using olive fruit extract and evaluation of their antibacterial and antioxidant properties. Front Chem. 2023;11; doi:10. 3389/fchem.2023.1202252
- [13] Assad N, Naeem-ul-Hassan M, Ajaz Hussain M, et al. Diffused sunlight assisted green synthesis of silver nanoparticles using Cotoneaster nummularia polar extract for antimicrobial and wound healing applications. Nat Prod Res. 2025;39(8):2203-2217. doi:10.1080/ 14786419.2023.2295936
- [14] Gilavand F, et al. Green synthesis of zinc nanoparticles using aqueous extract of Magnoliae officinalis and assessment of its bioactivity potentials. Biointerface Res Appl Chem. 2020;11(1):7765-7774.

- [15] Amin S, Sher M, Ali A, et al. Sulfonamide-functionalized silver nanoparticles as an analytical nanoprobe for selective Ni(II) sensing with synergistic antimicrobial activity. Environ Nanotechnol Monit Manage. 2022;18: 100735. doi:10.1016/j.enmm.2022.100735
- [16] Irfan MI, Amjad F, Abbas A, et al. Novel carboxylic acidcapped silver nanoparticles as antimicrobial and colorimetric sensing agents. Molecules. 2022;27(11):3363. doi:10.3390/molecules27113363
- [17] Mayegowda SB, et al. Green-synthesized nanoparticles and their therapeutic applications: a review. Green Process Synth. 2023;12(1). doi:10.1515/gps-2023-
- [18] Anjum S, Soliman MM, Althobaiti F, et al. Impacts of Ficus Religiosa-loaded chitosan nanoparticles against indomethacin induced peptic ulcer in rats: promising therapy with enhanced bioavailability and gastroprotective activity. Toxicol Res. 2025;14(3):tfaf034. doi: 10.1093/toxres/tfaf034
- [19] Liang J, He Y, Huang C, et al. The regulation of selenoproteins in diabetes: a new way to treat diabetes. Curr Pharm Des. 2024;30(20):1541-1547. doi:10.2174/0113 816128302667240422110226
- [20] Daniel AI, Umar MB, Tijani OJ, et al. Antidiabetic potentials of green-synthesized alpha iron oxide nanoparticles using stem extract of Securidaca longipedunculata. Int Nano Lett. 2022;12(3):281-293. doi:10.1007/s40089-022-00377-x
- [21] Shoaib A, Shahid S, Mansoor S, et al. Tailoring of an antidiabetic drug empagliflozin onto zinc oxide nanoparticles: characterization and in vitro evaluation of antihyperglycemic potential. Sci Rep. 2024;14(1):2499. doi: 10.1038/s41598-024-52523-4
- [22] Imraish A, Thiab TA, Zihlif M, et al. Anti-Inflammatory and antioxidant potential of green synthesized iron zinc oxide (Fe0.25-ZnO) nanoparticles of the Elaeagnus angustifolia. Chem Biodiversity. 2024;21(9):e20240 1060. doi:10.1002/cbdv.202401060
- [23] Jobe MC, et al. Biosynthesis of zinc oxide and silver/zinc oxide nanoparticles from Urginea epigea for antibacterial and antioxidant applications. Heliyon. 2022;8(12):e12243.
- [24] Robkhob P, Ghosh S, Bellare J, et al. Effect of silver doping on antidiabetic and antioxidant potential of ZnO nanorods. J Trace Elem Med Biol. 2020;58:126448. doi:10.1016/j.jtemb.2019.126448
- [25] Khafaga DSR, Eid MM, Mohamed MH, et al. Enhanced anticancer activity of silver doped zinc oxide magnetic nanocarrier loaded with sorafenib for hepatocel-Iular carcinoma treatment. Sci Rep. 2024;14(1):15538. doi:10.1038/s41598-024-65235-6
- [26] Feng C, Wang Y, Xu J, et al. Precisely tailoring molecular structure of doxorubicin prodrugs to enable stable nanoassembly, rapid activation, and potent antitumor effect. Pharmaceutics. 2024;16(12):1582. doi:10.3390/ pharmaceutics16121582
- [27] Yu J, Zhu F, Yang Y, et al. Ultrasmall iron-doped zinc oxide nanoparticles for ferroptosis assisted sonochemodynamic cancer therapy. Colloids Surf B. 2023; 232:113606. doi:10.1016/j.colsurfb.2023.113606
- [28] Dong Q, Jiang ZJI. Platinum-iron nanoparticles for oxygen-enhanced sonodynamic tumor cell suppression. Inorganics. 2024;12(12):331.
- [29] Anjum S, Khan A, Qamar A, et al. Light tailoring: impact of UV-C irradiation on biosynthesis, physiognomies, and clinical activities of morus macroura-mediated monometallic (Ag and ZnO) and bimetallic (Ag-ZnO)



- nanoparticles. Int J Mol Sci. 2021;22(20):11294. doi:10. 3390/ijms222011294
- [30] Nagvi SIZ, et al. Antifungal activity of juglans-regiamediated silver nanoparticles (AgNPs) against asper gillus-ochraceus-induced toxicity in in vitro and In vivo settings. J Funct Biomater. 2023;14(4):221.
- [31] Inam M, Haider Z, Anjum S, et al. Differential impact of biogenic and chemically synthesized zinc oxide nanoparticles on anti-aging, anti-oxidant and anticancerous activities: a mechanism based study. New J Chem. 2024;48(22):10161-10176. doi:10.1039/D4NJ0 1534G
- [32] Reyes-Pérez JA, Roa-Morales G, De León-Condes CA, et al. Nanocomposites from spent coffee grounds and iron/zinc oxide: green synthesis, characterization, and application in textile wastewater treatment. Water Sci Technol. 2023;88(6):1547–1563. doi:10.2166/wst.2023. 285
- [33] Faisal S, Jan H, Shah SA, et al. Green synthesis of zinc oxide (ZnO) nanoparticles using aqueous fruit extracts of myristica fragrans: their characterizations and biological and environmental applications. ACS Omega. 2021;6(14):9709-9722. doi:10.1021/acsomega.1c00310
- [34] Sohail MF, Rehman M, Hussain SZ, et al. Green synthesis of zinc oxide nanoparticles by neem extract as multi-facet therapeutic agents. J Drug Deliv Sci Technol. 2020;59:101911. doi:10.1016/j.jddst.2020.101911
- [35] Shah M, Nawaz S, Jan H, et al. Synthesis of biomediated silver nanoparticles from Silybum marianum and their biological and clinical activities. Mater Sci Eng C. 2020;112:110889. doi:10.1016/j.msec.2020.110889
- [36] Abbasi BH, Siddiquah A, Tungmunnithum D, et al. Isodon rugosus (wall. ex benth.) codd in vitro cultures: establishment, phytochemical characterization and in vitro antioxidant and anti-aging activities. Int J Mol Sci. 2019;20(2):452. doi:10.3390/ijms20020452
- [37] Apak R, Güçlü K, Özyürek M, et al. Novel total antioxidant capacity index for dietary polyphenols and vitamins C and E, using their cupric ion reducing capability in the presence of neocuproine: CUPRAC method. J Agric Food Chem. 2004;52(26):7970-7981. doi:10.1021/jf048741x
- [38] Meer B, Andleeb A, Iqbal J, et al. Bio-assisted synthesis and characterization of zinc oxide nanoparticles from lepidium sativum and their potent antioxidant, antibacterial and anticancer activities. Biomolecules. 2022;12(6):855. doi:10.3390/biom12060855
- [39] Nazir M, Tungmunnithum D, Bose S, et al. Differential production of phenylpropanoid metabolites in callus cultures of ocimum basilicum L. with distinct in vitro antioxidant activities and in vivo protective effects against UV stress. J Agric Food Chem. 2019;67(7):1847-1859. doi:10.1021/acs.jafc.8b05647
- [40] Khan AK, Renouard S, Drouet S, et al. Effect of UV irradiation (A and C) on casuarina equisetifoliamediated biosynthesis and characterization of antimicrobial and anticancer activity of biocompatible zinc oxide nanoparticles. Pharmaceutics. 2021;13(11):1977. doi:10.3390/pharmaceutics13111977
- [41] Berta L, Coman N-A, Rusu A, et al. A review on plantmediated synthesis of bimetallic nanoparticles, characterisation and their biological applications. Materials. 2021;14(24):7677. doi:10.3390/ma14247677
- [42] Alharbi NS, Alsubhi NS, Felimban Al. Green synthesis of silver nanoparticles using medicinal plants: characterization and application. J Radiat Res Appl Sci. 2022;15(3):109-124. doi:10.1016/j.jrras.2022.06.012

- [43] Kashkouli S, Jamzad M, Nouri A. Total phenolic and flavonoids contents, radical scavenging activity and green synthesis of silver nanoparticles by Laurus nobilis L. leaves aqueous extract. J Med Pl By-Products. 2018;7(1):25-32.
- [44] Benabdallah A, Rahmoune C, Boumendjel M, et al. Total phenolic content and antioxidant activity of six wild Mentha species (Lamiaceae) from northeast of Algeria. Asian Pac J Trop Biomed. 2016;6(9):760–766. doi:10.1016/j.apjtb.2016.06.016
- [45] Kyomuhimbo HD, et al. Silver-zinc oxide nanocomposite antiseptic from the extract of Bidens pilosa. SN Appl Sci. 2019;1:1-17.
- [46] Hosny M, Fawzy M, Eltaweil AS. Green synthesis of bimetallic Ag/ZnO@ Biohar nanocomposite for photocatalytic degradation of tetracycline, antibacterial and antioxidant activities. Sci Rep. 2022;12(1):7316. doi:10.1038/s41598-022-11014-0
- [47] Thatoi P, et al. Photo-mediated green synthesis of silver and zinc oxide nanoparticles using aqueous extracts of two mangrove plant species, Heritiera fomes and Sonneratia apetala and investigation of their biomedical applications. J Photochem Photobiol, B. 2016;163:311-318.
- [48] Akbar Jan F, Wajidullah, Ullah R, et al. Exploring the environmental and potential therapeutic applications of Myrtus communis L. assisted synthesized zinc oxide (ZnO) and iron doped zinc oxide (Fe-ZnO) nanoparticles. J Saudi Chem Soc. 2021;25(7):101278. doi:10.1016/j.jscs.2021.101278
- [49] Wei Y, Guo M. Zinc-binding sites on selected flavonoids. Biol Trace Elem Res. 2014;161(2):223-230. doi:10.1007/ s12011-014-0099-0
- [50] Usliyanage JP, Perera G, Thiripuranathar G, et al. Synthetic strategies of Aq-doped ZnO nanocomposites: a comprehensive review. Biomass Conver Biorefinery. 2025;15(1):19-39. doi:10.1007/s13399-023-05139-z
- [51] Boopathi TS, Suksom S, Suriyaprakash J, et al. Psidium guajava-mediated green synthesis of Fe-doped ZnO and Co-doped ZnO nanoparticles: a comprehensive study on characterization and biological applications. Bioprocess Biosyst Eng. 2024;47(8):1271-1291. doi:10.1007/s00449-024-03002-7
- [52] Ansar N, Shahid W, Irshad MA, et al. Aloe-inspired ecofriendly synthesis of Aq/ZnO heterostructures: boosting photocatalytic potential. Sci Rep. 2024;14(1):12711. doi:10.1038/s41598-024-61466-9
- [53] Carofiglio M, Laurenti M, Vighetto V, et al. Iron-Doped ZnO nanoparticles as multifunctional nanoplatforms for theranostics. Nanomaterials. 2021;11(10):2628. doi:10. 3390/nano11102628
- [54] Silambarasan M, Saravanan S, Soga T. Raman and photoluminescence studies of Ag and Fe-doped ZnO nanoparticles. Int J ChemTech Res. 2015;7(3):1644-1650.
- [55] Xu W, Yang T, Liu S, et al. Insights into the synthesis, types and application of iron nanoparticles: the overlooked significance of environmental effects. Environ Int. 2022;158:106980. doi:10.1016/j.envint.2021.106980
- [56] Asghari Moghaddam N, et al. Green synthesis of bimetallic AgZnO nanoparticles: synergistic anticancer effects through regulation of gene expression for lung cancer treatment. Results Eng. 2024;22:102329.
- [57] Craciun AM, Focsan M, Magyari K, et al. Surface plasmon resonance or biocompatibility - key properties for determining the applicability of noble metal nanoparticles. Materials. 2017;10(7):836. doi:10.3390/ma10070836



- [58] Guan R, Zhai H, Sun D, et al. Effects of Ag doping content and dispersion on the photocatalytic and antibacterial properties in ZnO nanoparticles. Chem Res Chin Univ. 2019;35(2):271-276. doi:10.1007/s40242-019-8275-6
- [59] Aiswarya Devi S, Harshiny M, Udaykumar S, et al. Strategy of metal iron doping and green-mediated ZnO nanoparticles: dissolubility, antibacterial and cytotoxic traits. Toxicol Res. 2017;6(6):854-865. doi:10.1039/ C7TX00093F
- [60] Ehsan M, Raja NI, Mashwani Z, et al. Responses of bimetallic Ag/ZnO alloy nanoparticles and urea on morphological and physiological attributes of wheat. IET Nanobiotechnol. 2021;15(7):602-610. doi:10.1049/ nbt2.12048
- [61] Ejaz A, Mamtaz Z, Yasmin I, et al. Cyperus scariosus extract based greenly synthesized gold nanoparticles as colorimetric nanoprobe for Ni2+ detection and as antibacterial and photocatalytic agent. J Mol Liq. 2024;393:123622. doi:10.1016/j.molliq.2023.123622
- [62] Riaz T, Mughal P, Shahzadi T, et al. Green synthesis of silver nickel bimetallic nanoparticles using plant extract of Salvadora persica and evaluation of their various biological activities. Mater Res Express. 2019;6(12):1250k3. doi:10.1088/2053-1591/ab74fc
- [63] Saeed F, Younas M, Fazal H, et al. Green and chemically synthesized zinc oxide nanoparticles: effects on in-vitro seedlings and callus cultures of Silybum marianum and evaluation of their antimicrobial and anticancer potential. Artif Cells Nanomed Biotechnol. 2021;49(1):450-460. doi:10.1080/21691401.2021. 1926274
- [64] Siddique AB, Amr D, Abbas A, et al. Synthesis of hydroxyethylcellulose phthalate-modified silver nanoparticles and their multifunctional applications as an efficient antibacterial, photocatalytic and mercury-selective sen sing agent. Int J Biol Macromol. 2024;256:128009. doi:10.1016/j.ijbiomac.2023.128009
- [65] Jabbar A, Abbas A, Assad N, et al. A highly selective Hg2+ colorimetric sensor and antimicrobial agent based on green synthesized silver nanoparticles using Equisetum diffusum extract. RSC Adv. 2023;13(41): 28666-28675. doi:10.1039/D3RA05070J
- [66] Zelekew OA, Haitosa HH, Chen X, et al. Recent progress on plant extract-mediated biosynthesis of ZnO-based nanocatalysts for environmental remediation: challenges and future outlooks. Adv Colloid Interface Sci. 2023;317:102931. doi:10.1016/j.cis.2023.102931
- [67] Hussain A, Fiaz S, Almohammedi A, et al. Optimizing photocatalytic performance with Ag-doped ZnO nanoparticles: synthesis and characterization. Heliyon. 2024;10(15):e35725. doi:10.1016/j.heliyon.2024.e35 725
- [68] Raza A, et al. Green synthesis of ZnO nanoparticles and Ag-doped ZnO nanocomposite utilizing sansevieria trifasciata for high-performance asymmetric supercapacitors. ACS Omega. 2024;9(30):32444-32454.
- [69] Gudla UR, Suryanarayana B, Raghavendra V, et al. Optical and luminescence properties of pure, iron-doped, and glucose capped ZnO nanoparticles. Results Phys. 2020;19:103508. doi:10.1016/j.rinp.2020.103508
- [70] Wenjuan C, Xueming M. Structural, optical and magnetic properties of Fe-doped ZnO. J Phys: Conf Ser. 2009;152(1):012039.
- [71] Narendhran S. Synergistic effect of Fe and Co doped ZnO nanoparticles synthesized using Alpinia galanga against Candida parasilopsis. Zastita Materijala. 2024; 65(2):246-257. doi:10.62638/ZasMat1131

- [72] Mohammadi-Aghdam S, Bahraini F, Ghoreishi SM. In-vitro anticancer on acute lymphoblastic leukemia NALM-6 cell line, antibacterial and catalytic performance of eco-friendly synthesized ZnO and Ag-doped ZnO nanoparticles using Hedera colchica extract. Bio mass Conversion and Biorefinery. 2024;14(17):20037-20052. doi:10.1007/s13399-023-04562-6
- [73] Hassan SS, Hassan AK, Abdul HMM. Green and chemical synthesis of bimetallic nanoparticles (Fe/Ni) supported by zeolite 5A as aheterogeneous fenton-like catalyst and study of kinetic and thermodynamic reaction for decolorization of reactive red 120 dye from aqueous pollution. Eurasian Chemical Communications. 2022;4(11):1062-1086.
- [74] Puthukkara PAR, Jose TS, Lal SD. Plant mediated synthesis of zero valent iron nanoparticles and its application in water treatment. Journal of Environmental Chemical Engineering. 2021;9(1):104569. doi:10.1016/j.jece.2020. 104569
- [75] E-08, A., Standard test method for analysis of hemolytic properties of nanoparticles. (2013). ASTM International West Conshohocken, PA.
- [76] Xu M, Niu Z, Liu C, et al. Oxidative potential of metalcontaining nanoparticles in coal fly ash generated from coal-fired power plants in China. Environment & Health. 2023;1(3):180-190. doi:10.1021/envhealth.3c00040
- [77] Mohanty S, Bharadwaj T, Verma D, et al. Development of Ag doped ZnO nanostructure and tranexamic acid infused chitosan-guargum film: a multifunctional antimicrobial dressing with haemostatic and wound closure potential. Chem Eng J. 2023;472:144976. doi:10.1016/j.cej.2023.144976
- [78] Yu M, Wu H, Meng Y, et al. Comprehensive biosafety assessment of Ag-ZnO/talc nanomaterials: implications for antibacterial applications. Appl Clay Sci. 2023;246:107185. doi:10.1016/j.clay.2023.107185
- [79] Muhideen Badhusha MS, Joel C, Imran Khan R, et al. Green synthesis and characterization of Fe doped ZnO nanoparticles and their interaction with bovine serum albumin. J Indian Chem Soc. 2021;98(11):100197. doi:10.1016/j.jics.2021.100197
- [80] Verma A, Stellacci F. Effect of surface properties on nanoparticle-cell interactions. Small. 2010;6(1):12-21. doi:10.1002/smll.200901158
- [81] Klein J. Probing the interactions of proteins and nanoparticles. Proc Natl Acad Sci U S A. 2007;104(7): 2029-2030. doi:10.1073/pnas.0611610104
- [82] Hanafy BI, Cave GWV, Barnett Y, et al. Nanoceria prevents glucose-induced protein glycation in eye lens cells. Nanomaterials. 2021;11(6):1473. doi:10.3390/ nano11061473
- [83] Ahmad S, Khan MS, Alouffi S, et al. Gold nanoparticlebioconjugated aminoguanidine inhibits glycation reaction: an in vivo study in a diabetic animal model. BioMed Res Int. 2021;2021:5591851. doi:10.1155/2021/5591
- [84] Sarmah S, Roy AS. A review on prevention of glycation of proteins: potential therapeutic substances to mitigate the severity of diabetes complications. Int J Biol Macromol. 2022;195:565-588. doi:10.1016/j.ijbiomac.2021. 12.041
- [85] Sadowska-Bartosz I, Bartosz G. Prevention of protein glycation by natural compounds. Molecules. 2015; 20(2):3309-3334. doi:10.3390/molecules20023309
- [86] Wei Y, Xu S, Wu Z, et al. Exploring the causal relationships between type 2 diabetes and neurological disorders using a Mendelian randomization strategy.

- - Medicine. 2024;103(46):e40412. doi:10.1097/MD.0000 000000040412
- [87] Kajaria D, Ranjana, Tripathi J, et al. In-vitro α amylase and glycosidase inhibitory effect of ethanolic extract of antiasthmatic drug - Shirishadi. J Adv Pharm Technol Res. 2013;4(4):206-209. doi:10.4103/2231-4040.121415
- [88] Sher N, Ahmed M, Mushtaq N, et al. Antioxidant, antidiabetic, and anti-Alzheimer performance of green synthesized silver, gold, and silver/gold bimetallic nanoparticles. Appl Organomet Chem. 2023;37(9):e7208. doi:10. 1002/aoc.7208
- [89] Jini D, Sharmila S, Anitha A, et al. In vitro and in silico studies of silver nanoparticles (AgNPs) from allium sativum against diabetes. Sci Rep. 2022;12(1):22109. doi:10.1038/s41598-022-24818-x
- [90] Wu Z, Zhang B, Yan B. Regulation of enzyme activity through interactions with nanoparticles. Int J Mol Sci. 2009;10(10):4198-4209. doi:10.3390/ijms10104198
- [91] Shejawal KP, Randive DS, Bhinge SD, et al. Green synthesis of silver and iron nanoparticles of isolated proanthocyanidin: its characterization, antioxidant, antimicrobial, and cytotoxic activities against COLO320DM and HT29. J Genet Eng Biotechnol. 2020;18(1):43. doi:10.1186/s43141-020-00058-2
- [92] Valgimigli L, Baschieri A, Amorati R. Antioxidant activity of nanomaterials. J Mater Chem B. 2018;6(14):2036-2051. doi:10.1039/C8TB00107C
- [93] Bhanja SK, et al. Green synthesis of Ag@Au bimetallic composite nanoparticles using a polysaccharide extracted from Ramaria botrytis mushroom and performance in catalytic reduction of 4-nitrophenol and antioxidant, antibacterial activity. Environ Nanotechnol Monit Manag. 2020;14:100341.
- [94] Samrot AV, Ram Singh SP, Deenadhayalan R, et al. Nanoparticles, a double-edged sword with oxidant as well as antioxidant properties - a review. Oxygen. 2022;2(4):591-604. doi:10.3390/oxygen2040039
- [95] Baschieri A, Ajvazi MD, Tonfack JLF, et al. Explaining the antioxidant activity of some common nonphenolic components of essential oils. Food Chem. 2017;232:656–663. doi:10.1016/j.foodchem.2017.04.
- [96] Thao NTM, et al. Antioxidant nanozymes: mechanisms, activity manipulation, and applications. Micromachines. 2023;14(5):1017.
- [97] Celardo I, Pedersen JZ, Traversa E, et al. Pharmacological potential of cerium oxide nanoparticles. Nanoscale. 2011;3(4):1411-1420. doi:10.1039/c0nr00875c
- [98] Nelson BC, et al. Antioxidant cerium oxide nanoparticles in biology and medicine. Antioxidants. 2016;5(2):15.
- [99] Lee J-W, Yoon S, Lo YM, et al. Intrinsic polyphenol oxidase-like activity of gold@platinum nanoparticles. RSC Adv. 2015;5(78):63757-63764. doi:10.1039/C5RA 07636F
- [100] Huang Y, Liu C, Pu F, et al. A GO-Se nanocomposite as an antioxidant nanozyme for cytoprotection. Chem Commun. 2017;53(21):3082-3085. doi:10.1039/C7CC00 045F
- [101] Hayyan M, Hashim MA, AlNashef IM. Superoxide ion: generation and chemical implications. Chem Rev. 2016; 116(5):3029-3085. doi:10.1021/acs.chemrev.5b00407
- [102] Brand MD, Affourtit C, Esteves TC, et al. Mitochondrial superoxide: production, biological effects, and activation of uncoupling proteins. Free Radical Biol Med. 2004;37(6):755-767. doi:10.1016/j.freeradbiomed. 2004.05.034

- [103] Huang Y, Liu Z, Liu C, et al. Self-assembly of multinanozymes to mimic an intracellular antioxidant defense system. Angew Chem. 2016;55(23):6646-6650. doi:10.1002/anie.201600868
- [104] Carofiglio M, Conte M, Racca L, et al. Synergistic phenomena between iron-doped ZnO nanoparticles and shock waves exploited against pancreatic cancer cells. ACS Appl Nano Mater. 2022;5(11):17212-17225. doi:10.1021/acsanm.2c04211
- [105] Tang Q, Xia H, Liang W, et al. Synthesis and characterization of zinc oxide nanoparticles from Morus nigra and its anticancer activity of AGS gastric cancer cells. J Photoch Photobio B. 2020;202:111698. doi:10.1016/j.jphotobiol.2019.111698
- [106] Ragab EM, El Gamal DM, Mohamed TM, et al. Impairment of electron transport chain and induction of apoptosis by chrysin nanoparticles targeting succinateubiquinone oxidoreductase in pancreatic and lung cancer cells. Genes Nutr. 2023;18(1):4. doi:10.1186/s12263-023-00723-4
- [107] Khalil AT, Ovais M, Ullah I, et al. Sageretia thea (Osbeck.) mediated synthesis of zinc oxide nanoparticles and its biological applications. Nanomedicine. 2017;12(15):1767-1789. doi:10.2217/nnm-2017-0124
- [108] Xia T, Zhao Y, Sager T, et al. Decreased dissolution of ZnO by iron doping yields nanoparticles with reduced toxicity in the rodent lung and zebrafish embryos. ACS Nano. 2011;5(2):1223-1235. doi:10.1021/nn1028 482
- [109] Zhang C, Liu Z, Zhang Y, et al. "Iron free" zinc oxide nanoparticles with ion-leaking properties disrupt intracellular ROS and iron homeostasis to induce ferroptosis. Cell Death Dis. 2020;11(3):183. doi:10.1038/s41419-020-
- [110] Wang D, Wu S, Fang J. Anticancer activity of zinc-nickel nanocomposite in lung cancer PC14 cells via modulation of apoptosis and P13 K/mTOR pathway. Arab J Chem. 2023;16(12):105318. doi:10.1016/j.arabjc.2023. 105318
- [111] Zheng Z, et al. Mechanisms and applications of radia tion-induced oxidative stress in regulating cancer immunotherapy. Frontiersin Immunol. 2023;4(14): 1247268.
- [112] Hu Y-B, Dammer EB, Ren R-J, et al. The endosomallysosomal system: from acidification and cargo sorting to neurodegeneration. Transl Neurodegener. 2015;4(1): 18. doi:10.1186/s40035-015-0041-1
- [113] Peña-Blanco A, García-Sáez AJ. Bax, bak and beyond - mitochondrial performance in apoptosis. FEBS J. 2018;285(3):416-431.
- [114] Dar MR, Khan AK, Inam M, et al. Differential impact of zinc salt precursors on physiognomies, anticancerous, and antibacterial activities of zinc oxide nanoparticles. Appl Biochem Biotechnol. 2024;196(8):4874-4899. doi:10.1007/s12010-023-04781-7
- [115] Ahmed W, Mansoor Q, Ahmad MS, et al. TRAIL mediated apoptosis ruling and anticancer trigger by finetuned nano spheres of Fagonia cretica methanolic extracts as novel cancer regime. Sci Rep. 2023;13(1):671. doi:10.1038/s41598-023-27441-6
- [116] Ma DD, Yang WX. Engineered nanoparticles induce cell apoptosis: potential for cancer therapy. Oncotarget. 2016;7(26):40882-40903. doi:10.18632/oncotarget.8553
- [117] Florance I, Cordani M, Pashootan P, et al. The impact of nanomaterials on autophagy across health and disease conditions. Cell Mol Life Sci. 2024;81(1):184. doi:10.1007/s00018-024-05199-y



- [118] Pimentel JM, Zhou JY, Wu GS. The role of TRAIL in apoptosis and immunosurveillance in cancer. Cancers. 2023;15(10):2752. doi:10.3390/cancers15102752
- [119] Mannoush SH, Jabir MS, Thaker AA. Gold and silica gold nanoparticles enhances macrophages kill tumor cells via granzyme-perforin pathway. Int J Health Sci. 2022;6(S6):8732-8745. doi:10.53730/ijhs.v6nS6. 12272